

Quantum field theory in curved graphene spacetimes, Lobachevsky geometry, Weyl symmetry, Hawking effect, and all that

Alfredo Iorio^{*}

*Faculty of Mathematics and Physics, Charles University in Prague, V Holešovičkách 2,
18000 Prague 8, Czech Republic*

Gaetano Lambiase[†]

*Department of Physics, University of Salerno, 84084-Fisciano (SA), Italy,
and INFN, Sezione di Napoli, Italy*

(Received 4 December 2013; revised manuscript received 23 May 2014; published 7 July 2014)

The solutions of many issues, of the ongoing efforts to make deformed graphene a tabletop quantum field theory in curved spacetimes, are presented. A detailed explanation of the special features of curved spacetimes, originating from embedding portions of the Lobachevsky plane into \mathbf{R}^3 , is given, and the special role of coordinates for the physical realizations in graphene is explicitly shown, in general, and for various examples. The Rindler spacetime is reobtained, with new important differences with respect to earlier results. The de Sitter spacetime naturally emerges, for the first time, paving the way to future applications in cosmology. The role of the Bañados, Teitelboim, and Zanelli (BTZ) black hole is also briefly addressed. The singular boundary of the pseudospheres, “Hilbert horizon,” is seen to be closely related to the event horizon of the Rindler, de Sitter, and BTZ kind. This gives new, and stronger, arguments for the Hawking phenomenon to take place. An important geometric parameter, c , overlooked in earlier work, takes here its place for physical applications, and it is shown to be related to graphene’s lattice spacing, ℓ . It is shown that all surfaces of constant negative curvature, $\mathcal{K} = -r^{-2}$, are unified, in the limit $c/r \rightarrow 0$, where they are locally applicable to the Beltrami pseudosphere. This, and $c = \ell$, allow us (a) to have a phenomenological control on the reaching of the horizon; (b) to use spacetimes different from the Rindler spacetime for the Hawking phenomenon; and (c) to approach the generic surface of the family. An improved expression for the thermal LDOS is obtained. A nonthermal term for the total LDOS is found. It takes into account (i) the peculiarities of the graphene-based Rindler spacetime; (ii) the finiteness of a laboratory surface; and (iii) the optimal use of the Minkowski quantum vacuum, through the choice of this Minkowski-static boundary.

DOI: 10.1103/PhysRevD.90.025006

PACS numbers: 11.30.-j, 04.62.+v, 72.80.Vp

I. INTRODUCTION

The intertwining between different branches of physics has always proven fruitful, from the Anderson [1] and Higgs [2] mechanisms to the now well established research on the gravity analogue systems (see, e.g., [3]). In recent years, this approach had a new boost with Maldacena’s discovery of the correspondence between certain gauge and gravity theories that goes under the generic name of AdS/CFT correspondence [4].

The results of this paper live at the crossroad of condensed matter and high energy theory. This research is carried out, mainly, as an attempt to construct with graphene a real system as close as possible to what is believed to be a quantum field in a curved spacetime. The task is difficult, but very much worthwhile. Positive outcomes can come on both sides.

As we shall recollect below, with graphene we have a quantum relativisticlike Dirac massless field available on a nearly perfectly two-dimensional sheet of carbon atoms. While this special-relativistic-like behavior of a condensed matter system is quite unusual (and it came as a surprise at the time of its discovery [5]), it is, by now, a well established experimental fact [6,7]. Building on our earlier work [8–11], the new direction we want to probe here is the emergence of gravitylike phenomena on graphene. In this paper, we give a detailed and extensive description of what needs to be done to see measurable effects of the quantum field theory (QFT) in a curved spacetime description of the electronic properties of graphene. We find here a number of new results that bring this goal closer.

The low-dimensional (two- and three-dimensional) setting is an extra bonus, as it points to the use of exact results, both on the field theory side and on the gravity side. Not least is the importance of Weyl symmetry [12] that points toward the use of conformally flat spacetimes [8]. One important issue, which we shall extensively deal with here,

^{*}alfredo.iorio@mff.cuni.cz

[†]lambiase@sa.infn.it

is that these spacetimes are in real terrestrial laboratories that, spatially, are \mathbf{R}^3 . For the sake of extracting measurable effects, such as a Hawking-Unruh effect, a crucial role will be played by surfaces of constant negative Gaussian curvature. It is well known that those surfaces can only be embedded into \mathbf{R}^3 at the price of essential singularities, as proven in a theorem by Hilbert [13–15]. We shall then have singularities all the time. We shall dedicate a big portion of this paper to elucidate these points. Although available in the mathematical literature, these results are rarely used in the context of QFT in curved spacetime because, there, n -dimensional spacetimes of constant negative curvature are usually seen as the result of embedding into a flat $(n + 1)$ -dimensional spacetime with signature $(+, -, \dots, +)$. Thus, when we point, for instance, to delicate constructions like the Bañados, Teitelboim, and Zanelli (BTZ) black hole [16] [besides the known subtleties of the global identifications that make an anti-de Sitter (AdS_3) spacetime a true black hole [17,18]], we have to keep in mind here that even the standard AdS_3 , to start with, is something to handle with care. Indeed, in a laboratory we are bound to a spacetime with signature $(+, -, -, -)$ where to embed the negative curvature spaces, and, in fact, we shall show that it is *de Sitter spacetime* that emerges more naturally. Furthermore, coordinates here have a more important status than in the customary proper relativistic setting, because the practical realization of this or the other reference frame is something we must care about.

Another crucial issue for the implementation on graphene of a sound QFT approach is that of the quantum vacuum. *The* distinctive feature of a quantum field is the excitation of particles out of the vacuum, through interactions, something impossible to describe within the formalism of quantum mechanics. In other words, in QFT, for both flat and curved spacetimes, there are choices of the ground state that are not equivalent, leading to (unitarily) inequivalent quantization schemes [19,20]. As is well known, this instance becomes central in QFT in curved spacetimes, where those inequivalent vacua are related to different observers, e.g., the inertial and the Kruskal observers of the Schwarzschild spacetime; see, e.g., [21–23]. That is at the core of the Hawking-Unruh effect: an observer in A sees the quantum vacuum in the frame B as a condensate of A particles. From preliminary results [24] we see that, on curved graphene, some kind of this nonequivalence is present, due to the topological disclination defects necessary for intrinsic curvature. Even though the system has finite degrees of freedom, defects introduce singularities in the domain of the Dirac operator; hence, through, e.g., the self-adjoint extension method [25], one can see inequivalent quantizations of the same topological nature as those appearing in the quantization of a particle on a circle [26]; see also [27].

There are other reasons to be careful with the choice of the quantum vacuum here. As just recalled, in standard

QFT in curved spacetimes one deals with various quantization schemes, each valid within a certain frame (say Minkowski and Rindler), but the field is always the same. The nature of the quantum field is not fundamentally changed in going from one frame to another. The notions of positive frequency, of vacuum, of creation and annihilation operators, etc., change [21], but we shall never end up with, say, a massive scalar field if we started with a massless spinor field. This obvious consideration does not apply to the field-theoretical description of graphene. The pseudoparticles only live on the graphene sheet; i.e., their existence is due to the structure of the lattice. So, after that “object” has left the graphene sample and has reached the outside world, its description changes dramatically. It turns into a massive, $(3 + 1)$ -dimensional, nonrelativistic (in the sense of c , speed of light) electron for which the whole description we are concerned about is gone forever. All of that needs to be taken into account in this hybrid approach, where pure QFT in curved spacetimes and condensed matter effective descriptions merge. The issue was faced in [9] and will be further addressed here. The solution we have found is to use, in all cases, the $(2 + 1)$ -dimensional Minkowski inertial vacuum, hence relativistic, but *in the sense of v_F , Fermi velocity*, as the reference vacuum for the computation of all Green functions.

Local Weyl symmetry will play an important role in this work. This is a symmetry of the massless Dirac action under transformations that, in $(2 + 1)$ dimensions, take the following form¹:

$$g_{\mu\nu}(x) \rightarrow \phi^2(x)g_{\mu\nu}(x) \quad \text{and} \quad \psi(x) \rightarrow \phi^{-1}(x)\psi(x); \quad (1)$$

note that all the quantities are computed at the same point x in spacetime.

To appreciate the physical meaning of this symmetry, it should be considered that it relates the physics in a given spacetime (metric $g_{\mu\nu}$) to the physics in a *different* spacetime (metric $\phi^2 g_{\mu\nu}$). For instance, when the background spacetime $g_{\mu\nu}$ is curved but conformally flat, since we can take advantage from the privileged link with the flat

¹Here are our notations: $\phi(x)$ is a scalar field (conformal factor), $\mu, \nu = 0, 1, \dots, n - 1$ are Einstein indices, responding to diffeomorphisms, $a, b = 0, 1, \dots, n - 1$ are flat indices, responding to local Lorentz transformations, while α, β are spin indices. The covariant derivative is $\nabla_\mu \psi_\alpha = \partial_\mu \psi_\alpha + \Omega_{\mu\alpha}^\beta \psi_\beta$ with $\nabla_a = E_a^\mu \nabla_\mu$, $\Omega_{\mu\alpha}^\beta = \frac{1}{2} \omega_\mu^{ab} (J_{ab})_\alpha^\beta$, where $(J_{ab})_\alpha^\beta$ are the Lorentz generators in spinor space, and $\omega_{\mu b}^a = e_\lambda^a (\partial_\mu^\lambda \partial_\mu + \Gamma_{\mu\lambda}^\lambda) E_b^\lambda$ is the spin connection, whose relation to the Christoffel connection comes from the metricity condition $\nabla_\mu e_\nu^a = \partial_\mu e_\nu^a - \Gamma_{\mu\nu}^\lambda e_\lambda^a + \omega_{\mu b}^a e_\nu^b = 0$. We also introduced the vielbein e_μ^a (and its inverse E_a^μ), satisfying $\eta_{ab} e_\mu^a e_\nu^b = g_{\mu\nu}$, $e_\mu^a E_a^\nu = \delta_\mu^\nu$, $e_\mu^a E_b^a = \delta_b^\mu$, where $\eta_{ab} = \text{diag}(1, -1, \dots)$. The Weyl dimension of the Dirac field ψ in n dimensions is $d_\psi = (1 - n)/2$. In this paper $n = 3$, and we can move one dimension up (embedding) or down (boundary). More on the notations is in [8,28].

spacetime counterpart, Weyl symmetry might allow for exact nonperturbative results in the computation of the Green functions [8], a very difficult task to accomplish by other means [21]. When we are dealing with a conformally invariant field in a conformally flat spacetime, this is sometimes referred to as *conformal triviality* [21], a name that emphasizes the simplest possible case of QFT in curved space, but, perhaps, does not do justice to the fact that the key features are indeed at work. If the spacetime is only curved in a conformally flat fashion, the effects of curvature are null on the *classical physics* of a massless Dirac field. To spot the effects of curvature we need to move to the *quantum regime*.

Another reason for considering conformally flat spacetimes is that, in this case, the chiral term mixing the two Dirac spinors, $\epsilon^{abc} \omega_{abc} (\bar{\psi}_+ \sigma_3 \psi_- + \bar{\psi}_- \sigma_3 \psi_+)$, is identically zero (see Sec. 2 and [28]).

A further reason for considering the conformally flat cases lies with the gravitational analogues of these settings. For instance, there are interesting configurations, such as the mentioned $(2+1)$ -dimensional BTZ black hole (see [29] for a study of graphene and the BTZ black hole that follows our approach) and the gravitational kink of [30], which are conformally flat configurations. For all these reasons, in this paper we shall almost entirely focus on the conformally flat cases. Nonetheless, many of the arguments presented here apply to the general case.

II. DIRAC FIELD DESCRIPTION OF DEFORMED GRAPHENE

Graphene is an allotrope of carbon. It is one atom thick; hence it is the closest in nature to a two-dimensional object. It was first theoretically speculated about [31,32] and, decades later, experimentally found [5]. The honeycomb lattice of graphene is made of two intertwined triangular sublattices; see Fig. 1. Of the carbon's four electrons available to form covalent bonds, three are put in common with the three nearest neighbors (one each), forming what

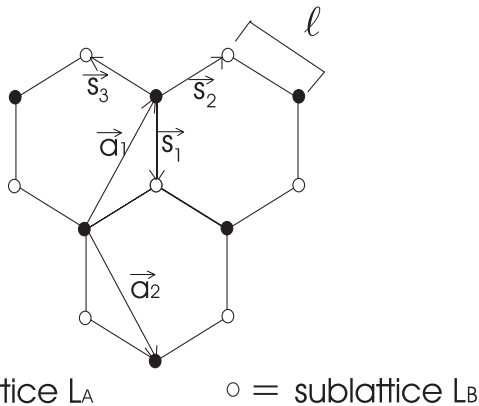


FIG. 1. Our choice for the basis vectors of the honeycomb graphene lattice.

are known as σ bonds (the molecular-level merging of the atomic $2s$ orbitals). These bonds are responsible for the *elastic properties* of the membrane. The fourth electron also forms a covalent bond, called the π bond, but only with one of the three neighbors. Furthermore, being the π orbitals of the molecular-level merging of the atomic $2p$ orbitals, it has nodes on the membrane, and the electrons there are much more free to “hop.” Thus, the latter bond (π) is of a much weaker kind than the former (σ). The *electronic properties* of graphene are due to the electrons belonging to the π orbitals.

In this paper we deal with the electrons of the π orbitals. Hence, although the effects of the deformations of the membrane will be duly taken into account, the elastic properties are not our direct concern. We shall propose various morphologies, for reasons that are on the theoretical side, but we shall not prove whether those shapes are elastically permitted or feasible from the practical/engineering point of view. On the other hand, we are not making impossible requests, because, graphene being the thinnest material in nature, it is reasonable to think that it might be forced to have a variety of shapes. Surely, suspended graphene's samples come with corrugations and ripples [33], and many deformations have been induced to study the effects of curvature and strain on the electronic properties, a central issue in the ongoing studies of graphene on the condensed matter side; see, e.g., [34]. Recalling that our main goal here is to show how graphene can be used to very effectively mimic a quantum field on a curved spacetime, the fact that we have to force a little the material in that direction comes as a fair price to pay. Furthermore, we shall make here the greatest effort, on the theoretical side, to simplify the requests for the occurrence of these exotic behaviors on graphene to “simply” curve the material in specific ways.

As is by now well known, graphene's lattice structure is behind a natural description of its electronic properties in terms of massless, $(2+1)$ -dimensional, Dirac (hence, relativisticlike) pseudoparticles [7]. In the honeycomb lattice, there are two inequivalent sites per unit cell, the white and black spots in Fig. 1, that do not refer to different atoms (they all are carbons) but to their topological inequivalence. Contrary to a square lattice, the basis vectors, (\vec{a}_1, \vec{a}_2) , are not enough to reach all the points (black and white), and an extra set of vectors, $(\vec{s}_1, \vec{s}_2, \vec{s}_3)$, is needed. That is how the two-component Dirac spinor emerges. Hence, the Dirac description is resistant to changes of the lattice that preserve this aspect of the structure. See, e.g., the developments in [35], where the authors discuss *graphyne*, by departing from the hexagonal structure but retaining the two inequivalent sites per unit cell, and hence the Dirac description. In \vec{k} space, the valence band and the conductivity band touch in two inequivalent points (we use $\hbar = 1$) $\vec{k}_{\pm}^D = (\pm \frac{4\pi}{3\sqrt{3}\ell}, 0)$, with

$\ell \simeq 1.4 \text{ \AA}$, and near those points the spectrum is *linear*, $E_{\pm} \simeq \pm v_F |\vec{k}|$, where $v_F = 3\eta\ell/2 \sim c/300$ is the Fermi velocity, with $\eta \simeq 2.8 \text{ eV}$ the nearest-neighbor hopping energy. This behavior is expected in a relativistic theory, whereas, in a nonrelativistic system, the dispersion relations are usually quadratic. Hence, if one linearizes around \vec{k}_{\pm}^D : $\vec{k}_{\pm} \simeq \vec{k}_{\pm}^D + \vec{p}$, one can write the Hamiltonian in terms of \vec{p} within the range given by

$$E_{\ell} \sim v_F/\ell \sim 4.2 \text{ eV}. \quad (2)$$

Notice that $E_{\ell} \sim 1.5\eta$ and that the associated wavelength, $\lambda = 2\pi/|\vec{p}| \simeq 2\pi v_F/E$, is $2\pi\ell$. The electrons' wavelength, at energies below E_{ℓ} , is large compared to the lattice length, $\lambda > 2\pi\ell$. Those electrons see the graphene sheet as a continuum; hence, over the whole linear regime, the following Hamiltonian well captures the physics:

$$H = -iv_F \int d^2x (\psi_+^{\dagger} \vec{\sigma} \cdot \vec{\partial} \psi_+ + \psi_-^{\dagger} \vec{\sigma}^* \cdot \vec{\partial} \psi_-), \quad (3)$$

where $\vec{\sigma} \equiv (\sigma_1, \sigma_2)$, $\vec{\sigma}^* \equiv (-\sigma_1, \sigma_2)$, with σ_i the Pauli matrices, and with $\psi_{\pm} \equiv (a_{\pm}, b_{\pm})^T$ the two-component Dirac spinors, as appropriate for this $(2+1)$ -dimensional system, and we are in configuration space, $\vec{p} \rightarrow -i\vec{\partial}$.

Long before the advent of graphene, a field theoretical Dirac approach has also been successfully put forward on “inflated” *buckyball fullerenes* [36] (carbon structures that can be thought of as graphene sheets, warped to make spheres). Later, this approach was extended to *curved graphene*; see, e.g., Ref. [37], where spatial curvatures in this Dirac field theoretical model were taken into account. Those can surely be taken as pioneering steps towards a QFT in curved spacetimes description of the electronic properties of graphene. Nonetheless, as recalled earlier, the distinctive features of a quantum field in curved spacetimes are as follows: the role of the nontrivial vacua, their relation to different quantization schemes for different observers, and a full inclusion of the time in a relativistic-like description. Each of the above finds its synthesis in the Unruh or the Hawking effects, which to many (see, e.g., [38]) are the clearest and unmistakable experimental signature of QFT in curved spacetime. That is the road pursued in [9], which we want to pursue further here.

To include time in a more democratic fashion, let us consider the action, rather than the Hamiltonian [8]

$$A = v_F \int d^3x (i\psi^{\dagger} \dot{\psi} - \mathcal{H}) = iv_F \int d^3x \bar{\psi} \gamma^a \partial_a \psi, \quad (4)$$

where $x^0 \equiv v_F t$ and the γ matrices, $\gamma^0 = \sigma_3$, $\gamma^1 = i\sigma_2$, $\gamma^2 = -i\sigma_1$, obey all the standard properties, e.g., $[\gamma^a, \gamma^b]_{+} = 2\eta^{ab}$ (see [28]). Notice that, as we do not consider phenomena mixing the two Fermi points, we focus on a single one, hence, say, $\psi \equiv \psi_{+}$.

Besides the scale introduced above, we also have a second scale. When we introduce intrinsic curvature, E_{ℓ} is beyond our reach. It is our “high energy regime.” This is so because we ask the curvature to be small compared to a limiting maximal curvature, $1/\ell^2$, otherwise (i) it would make no sense to consider a smooth metric, and (ii) $r < \ell$ (where $1/r^2$ measures the intrinsic curvature) means that we should bend the very strong σ bonds, an instance that does not occur. Therefore, our second reference energy is

$$E_r \sim v_F/r, \quad (5)$$

with $E_r = \ell/r E_{\ell} < E_{\ell}$. Taking, e.g., $r \simeq 10\ell$ as a small radius of curvature (high intrinsic curvature), this energy is $E_r \sim 0.4 \text{ eV}$, while for $r \sim 1 \text{ mm} \sim 10^6 \ell$, $E_r \sim 0.6 \mu \text{ eV}$. Energies below E_r are our “low energy regime.” The considerations of this paper apply there.

To find the action that, when the graphene membrane is deformed, well captures the physics of the electrons in the π bonds with very large wavelengths ($\lambda > 2\pi r$), we need to know how possible deformations can be encoded within the Dirac field formalism. As we are in a weak scatterers regime [39,40], where the Born approximation is valid,² there are three kinds of deformation that can still be at work [7]: intrinsic curvature, extrinsic curvature, and strain. The intrinsic curvature is clearly an *inelastic* deformation of the lattice. This is customarily described in elasticity theory (see, e.g., [41,42]) by the (smooth) derivative of the (noncontinuous) SO(2)-valued rotational angle $\partial_i \omega \equiv \omega_i$, where $i = 1, 2$ is a curved spatial index (see footnote 1 for notation on indices, etc.). The corresponding (spatial) Riemann curvature tensor is easily obtained,

$$R^{ij}{}_{kl} = e^{ij} \epsilon_{kl} e^{mn} \partial_m \omega_n = e^{ij} \epsilon_{lk} 2\mathcal{K}, \quad (6)$$

where \mathcal{K} is the Gaussian (intrinsic) curvature of the surface. In our approach we include time, although the metric we shall adopt is

$$g_{\mu\nu}^{\text{graphene}} = \begin{pmatrix} 1 & 0 & 0 \\ 0 & & \\ 0 & g_{ij} & \end{pmatrix}; \quad (7)$$

i.e., the curvature is all in the spatial part, and $\partial_t g_{ij} = 0$. Since the time dimension is included, the SO(2)-valued (Abelian) disclination field has to be lifted up to a SO(1,2)-valued (non-Abelian) disclination field,³ ω_{μ}^a , $a = 0, 1, 2$, with $\omega_{\mu}^a = e_{\mu}^b \omega_b^a$, and the expression

$$\omega_a^d = \frac{1}{2} e^{bcd} (e_{\mu a} \partial_b E_c^{\mu} + e_{\mu b} \partial_a E_c^{\mu} + e_{\mu c} \partial_b E_a^{\mu}) \quad (8)$$

²On these points, we greatly benefited from correspondence with Paco Guinea.

³Recall that in three dimensions $\omega_{\mu ab} = \epsilon_{abc} \omega_{\mu}^c$.

gives the relation between the disclination field and the metric (dreibein). All the information about intrinsic curvature does not change. For instance, the Riemann curvature tensor, $R^\lambda{}_{\mu\nu\rho}$, has only one independent component, proportional to \mathcal{K} , just as in (6) (see [8]). What we gain here is the possibility to use a full relativistic approach where, for instance, a change of frame (or the inclusion of an external potential, mimicking the gravitational potential) might change g_{00} in (7). In the next sections we shall exploit these features.

Notice that different methods of preparation of the samples lead to different defect concentrations, and, even if the lattice effects can be neglected at these wavelengths, if defects are too highly concentrated we cannot assume a smoothly curved metric as that in (7) to describe this situation. We shall then assume that the defects are homogeneously distributed, and not too much concentrated to avoid interactions among defects. This is yet another reason not to consider too big curvatures (the density of defects per unit area grows with r^{-2}).

Summarizing, the effects of intrinsic curvature on the electronic properties of graphene can be included, within the Dirac description, through the substitution

$$\partial_\mu \rightarrow \partial_\mu + \Omega_\mu, \quad (9)$$

with $\Omega_\mu \equiv \omega_\mu^a J_a$, and J_a the generators of $\text{SO}(1,2)$, the local Lorentz transformations (see [28] for details). On the gauge field approach, see, e.g., [43].

The other two deformations are elastic, and, in this paper, we are looking for the effects of intrinsic curvature. Thus, as clarified in the previous paragraphs, we have to focus on electrons with very large wavelengths, and our energies range only up to E_r . For these energies, the inelastic effects will dominate over the elastic ones, but, by focusing only on the former it is an approximation. As such, in an experiment, we might see the effects of these strain-induced fields; see, e.g., [44,45]. Work is in progress to duly describe also purely elastic deformations, within the Weyl symmetry approach [46].

With this in mind, the very long wavelength/very small energy electronic properties of graphene are well described by the following action:

$$A = iv_F \int d^3x \sqrt{g} \bar{\psi} \gamma^\mu (\partial_\mu + \Omega_\mu) \psi, \quad (10)$$

which we shall use from now on.

While, of course, the \sqrt{g} needs be there for a diffeomorphic covariant action in the presence of curvature, and hence it would need no further justification, our construction of (10) entirely from graphene-related quantities might appear incomplete if we do not justify this factor too. Indeed, this factor, combined with the constant v_F , can give rise to a space dependent Fermi

velocity⁴ $v_F(x)$. This feature also emerges from a pure tight-binding computation [47], and it is further considered in [46].

One last issue needs to be mentioned before proceeding. We are focusing on phenomena that do not mix the two Fermi points, and, in general, curvature could spoil that by producing a chiral term in the action. This term would take into account well-known features of graphene with $(2n+1)$ -folded disclination defects. In those cases, because of a flipping along the dislocation line, one needs to take into account both Fermi points. This is better seen in the four component Dirac spinor language, where the two Dirac points are treated at once. That way one obtains a chiral term in the action of the form

$$A_\chi = \frac{1}{4} \int d^3x \sqrt{g} \epsilon^{abc} \omega_a{}_{bc} (\bar{\psi}_+ \sigma_3 \psi_- + \bar{\psi}_- \sigma_3 \psi_+). \quad (11)$$

Nonetheless, we take advantage from the fact that this term is identically zero for the conformally flat case of interest here. Indeed, it can be proved that the total number of “flipping” dislocation lines is even in the ideal case. Hence, when all the surface is considered, the total effect is gone. In the continuous metric language, this is seen by noticing that, when $g_{\mu\nu} = \phi^2 \eta_{\mu\nu}$, one has $\omega_{\mu bc} = \delta_\mu^a (\eta_{ab} \delta_c^b - \eta_{ac} \delta_b^c) (\partial_\nu \ln \phi)$. This approximation can also affect the experiments when the observables are measured along the dislocation lines. On all this see [28].

III. MERGING CURVED GRAPHENE AND QFT IN CURVED SPACETIMES

Bearing in mind the previous discussion, to extract experimental predictions from the hypothesis that graphene conductivity electrons realize a quantum field on a curved background, described by the action (10), we proceed as follows.

First of all, we focus on surfaces of constant \mathcal{K} . As recalled at the end of the Introduction, and as explained in [8], to make the most of the Weyl symmetry of (10), we better focus on conformally flat metrics. The simplest metric to obtain in a laboratory is of the kind (7). For this metric the Ricci tensor is $R_\mu{}^\nu = \text{diag}(0, \mathcal{K}, \mathcal{K})$. This gives, as the only nonzero components of the Cotton tensor, $C^{\mu\nu} = \epsilon^{\mu\sigma\rho} \nabla_\sigma R_\rho{}^\nu + \mu \leftrightarrow \nu$, the result $C^{0x} = -\partial_y \mathcal{K} = C^{x0}$ and $C^{0y} = \partial_x \mathcal{K} = C^{y0}$. Since conformal flatness in $(2+1)$ dimensions amounts to $C^{\mu\nu} = 0$, this shows that all surfaces of constant \mathcal{K} give rise in (7) to conformally flat $(2+1)$ -dimensional spacetimes [note that the result holds for

⁴For instance, for a conformally flat spacetime, $g_{\mu\nu} = \phi^2 \eta_{\mu\nu}$; hence $\sqrt{g} = \phi^3$. Considering $\psi = \phi^{-1} \psi'$ [see (1)], a rough estimate in (10) gives $v_F(x) \sim \phi^3 \phi^{-2} v_F = \phi(x) v_F$, which is in agreement with the more sophisticated results we shall obtain later.

(+, −, −) and for (+, +, +)]. This means that we focus on *surfaces of constant Gaussian curvature*.

The result $C^{\mu\nu} = 0$ is intrinsic (it is a tensorial equation, true in any frame), but to exploit Weyl symmetry to extract nonperturbative exact results, we need to find the coordinate frame, say $Q^\mu \equiv (T, X, Y)$, where

$$g_{\mu\nu}^{\text{graphene}}(Q) = \phi^2(Q)g_{\mu\nu}^{\text{flat}}(Q). \quad (12)$$

Here, besides the technical problem of finding these coordinates, the issue is as follows: *what is the physical meaning of the coordinates Q^μ and their practical feasibility*.

Tightly related to the previous point is the issue of a conformal factor that makes the model *globally predictive, over the whole surface/spacetime*. The simplest possible solution would be a single-valued and time independent $\phi(q)$, already in the original coordinates frame, $q^\mu \equiv (t, u, v)$, where t is the laboratory time, and, e.g., u, v the meridian and parallel coordinates of the surface.

Here we are dealing with a spacetime that is embedded into the flat (3 + 1)-dimensional Minkowski. Although, as said, we shall focus on intrinsic curvature effects, just as in a general relativistic context, issues related to the embedding, even just for the spatial part, are important. For instance, when the surface has negative curvature, we need to move from *the abstract objects of non-Euclidean geometry* (say the coordinates of the upper-half plane model of Lobachevsky geometry) *to objects measurable in a Euclidean real laboratory*. This will involve the last issue above about global predictability and, in the case of negative curvature, will necessarily lead to singular boundaries for the surfaces, as proved in a theorem by Hilbert; see, e.g., [15,38,48]. Even the latter fact is, in a sense, a coordinates effect, due to our insisting on embedding in \mathbf{R}^3 , and it clarifies the hybrid nature of these pseudorelativistic settings. Nonetheless, once we are in \mathbf{R}^3 , there is no way to remove such singularities; we can only relocate them by changing the surface (see later).

We then need to find the *quantum vacuum of the field* to properly take into account the following: (a) *the measurements*, as for any QFT on a curved spacetime, and (b) *the graphene hybrid situation*. As is well known, in QFT, in general, we have choices of the ground states that are not equivalent; i.e., they are not connected through a non-singular unitary transformation [19,20]. This instance becomes particularly important in QFT in curved spacetimes, where those inequivalent vacua are related to different observers; see, e.g., [21–23].

Having in mind that the clearest prediction of QFT on a curved spacetime is the *Hawking effect*, if we want to prove beyond doubt that graphene realizes such a system, we shall have to face the challenge to reproduce on graphene the conditions for this effect to take place. Thus, one of the main challenges is to realize the conditions for which an

event horizon appears. Having confined ourselves to metrics of the kind (7) the task is indeed a difficult one, and, since we shall focus on surfaces of constant negative \mathcal{K} , we have to face the fact that the surface might end before the horizon is reached; see [29]. In [9], for one specific case, and in the following, for more cases, we show that these problems can be solved.

Of course, we do not argue that this procedure is the only one leading to an experimental test of the validity of the QFT in a curved spacetime description of the physics of graphene’s π bonds. One could depart from the beginning from the metric (7), for instance by applying external electromagnetic fields, or imagining more or less exotic situations where the $g_{00} \neq 1$. Nonetheless, acting as explained above merges two goals: to be experiments friendly, and to keep on board as many as possible of the crucial aspects of QFT in curved spacetimes.

Let us now face all the issues of this list, starting from the first set, i.e., what we might call the “geometric” and the “relativity” issues.

IV. THE GEOMETRIC ISSUES: LOBACHEVSKY GEOMETRY IN THE LAB

Our focus will be on the surfaces of constant Gaussian curvature, one of the subject matters of the classic studies of differential geometry [13,49]. Let us recall here the main facts about them that we shall need in the following.

In general, there is no single parametrization good for all surfaces. In fact, for the surfaces of revolution, there is one such parametrization, sometimes called “canonical,” that we now introduce. Surfaces of revolution are the surfaces swapped by a (profile) curve, say in the plane (x, z) , rotated of a full angle around the z axis. All such surfaces (both of constant and nonconstant \mathcal{K}) can be parametrized in \mathbf{R}^3 as

$$\begin{aligned} x(u, v) &= R(u) \cos v, & y(u, v) &= R(u) \sin v, \\ z(u) &= \pm \int^u \sqrt{1 - R'^2(\bar{u})} d\bar{u}, \end{aligned} \quad (13)$$

where the prime denotes the derivative with respect to the argument, $v \in [0, 2\pi]$ is the parallel coordinate (angle), and u is the meridian coordinate whose range is fixed by the knowledge of $R(u)$, i.e., of the type of surface, through the request that $z(u) \in \mathbf{R}$. The relation between z and R comes from the constraint $R'^2(u) + z'^2(u) = 1$, which amounts to a choice (that we are free to make) for the coefficients of Gauss’s first fundamental form given by [49] $E = 1$, $F = 0$, $G = R(u)$. A direct proof of this last statement is obtained by considering the embedded line element descending from (13),

$$dl^2 \equiv dx^2 + dy^2 + dz^2 = du^2 + R^2(u)dv^2. \quad (14)$$

The expression on the far right side above is the typical line element of a surface of revolution. We shall always deal

with such type of line element, for the spatial part. The way the surface of revolution can be plotted via the line element (14) is by drawing successive circular ($v \in [0, 2\pi]$) slices of varying radii $R(u)$.

The Gaussian curvature is given by the simple expression [49]

$$\mathcal{K} = -\frac{R''(u)}{R(u)}. \quad (15)$$

Thus, the knowledge of $R(u)$ amounts to the knowledge of the surface of revolution. When \mathcal{K} is constant, Eq. (15) is an easy equation to solve

$$R(u) = c \cos(u/r + b) \quad \text{for} \quad \mathcal{K} = \frac{1}{r^2}, \quad (16)$$

$$R(u) = c_1 \sinh(u/r) + c_2 \cosh(u/r) \quad \text{for} \quad \mathcal{K} = -\frac{1}{r^2}, \quad (17)$$

where $r \in \mathbf{R}$ is constant, and c, b, c_1, c_2 are also real constants that determine the type of surface, and/or set the zero and scale of the coordinates.

When $\mathcal{K} = 1/r^2$, one first chooses the zero of u in such a way that b in (16) is zero, and then distinguishes three cases, $c = r$, $c > r$, $c < r$. The first case is the sphere of radius r , and the other two surfaces are applicable to the sphere through a redefinition of the

meridian coordinate $v \rightarrow (c/r)v$. With these, $z(u) = \int^u \sqrt{1 - (c^2/r^2) \sin^2(\bar{u}/r)} d\bar{u}$, and the range of u changes according to the relation between c and r , being $z(u) = r \sin(u/r)$, with $u/r \in [-\pi/2, +\pi/2]$ for the sphere.

When $\mathcal{K} = -1/r^2$, all the surfaces described by (17) can be applied to one of the following three cases: $c_1 = c_2 \equiv c$, giving

$$R(u) = ce^{u/r}, \quad (18)$$

or $c_1 = 0, c_2 \equiv c$, giving

$$R(u) = c \cosh(u/r), \quad (19)$$

or $c_2 = 0, c_1 \equiv c$, giving

$$R(u) = c \sinh(u/r). \quad (20)$$

They are called the *Beltrami*, the *hyperbolic*, and the *elliptic* pseudospheres, respectively, and the corresponding expressions for $z(u)$ are given by substituting $R(u)$ in the integral in (13). Very important for us, *all surfaces* of constant negative \mathcal{K} , not only the surfaces of revolution, are applicable to the Beltrami or the hyperbolic or the elliptic pseudospheres; see, e.g., [13].

The condition $z \in \mathbf{R}$ gives the range of R and u in the various cases

$$R(u) \in [0, r] \Leftrightarrow u \in [-\infty, r \ln(r/c)], \quad (21)$$

$$R(u) \in [c, \sqrt{r^2 + c^2}] \Leftrightarrow u \in [-\operatorname{arccosh}(\sqrt{1 + r^2/c^2}), +\operatorname{arccosh}(\sqrt{1 + r^2/c^2})], \quad (22)$$

$$R(u) \in [0, r \cos \vartheta] \Leftrightarrow u \in [0, \operatorname{arcsinh} \cot \vartheta], \quad (23)$$

where, in the first two cases, c is only bound to be a real positive number, while in the last case $0 < c = r \sin \vartheta < r$. Furthermore, in the second case, $R(u)$ is an even function of u , and hence, in the symmetric interval, reaches the maximum twice. Notice also that the only case where the range of R is independent from c is for the Beltrami surface. More details of these surfaces are in the captions of the relative figures; see Figs. 3, 4, and 5 below.

On the mathematics side, our goal is to find the coordinate frame $Q^\mu \equiv (T, X, Y)$ where the metric (7) is explicitly conformally flat. On the physics side, we have to understand what are the conditions that need to be realized on graphene to correspond to this frame, and how feasible this is.

One problem to solve, on the spatial part, is to combine the canonical parametrization (13), for which it is immediate to plot the surface, with the spatial isothermal

coordinates, (\tilde{x}, \tilde{y}) , where $dl^2 = \varphi^2(\tilde{x}, \tilde{y})(d\tilde{x}^2 + d\tilde{y}^2)$, where the task to find the coordinate frame Q^μ is easier. Indeed,

$$g_{\mu\nu}^{\text{graphene}} = \operatorname{diag}(1, -\varphi^2(\tilde{x}, \tilde{y}), -\varphi^2(\tilde{x}, \tilde{y})) \\ = \varphi^2(T, X, Y) \operatorname{diag}(1, -1, -1); \quad (24)$$

hence, using the standard $g_{\mu\nu}(Q) = (\partial Q_\mu / \partial q_\lambda) \times (\partial Q_\nu / \partial q_\kappa) g_{\lambda\kappa}(q)$, the system of partial differential equations to solve simplifies to

$$\begin{aligned} \phi^2(T_t^2 - X_t^2 - Y_t^2) &= 1, \\ \phi^2(T_{\tilde{y}}^2 - X_{\tilde{y}}^2 - Y_{\tilde{y}}^2) &= -\varphi^2 = \phi^2(T_{\tilde{x}}^2 - X_{\tilde{x}}^2 - Y_{\tilde{x}}^2), \quad (25) \\ T_t T_{\tilde{x}} - X_t X_{\tilde{x}} - Y_t Y_{\tilde{x}} &= T_t T_{\tilde{y}} - X_t X_{\tilde{y}} - Y_t Y_{\tilde{y}} \\ &= T_{\tilde{x}} T_{\tilde{y}} - X_{\tilde{x}} X_{\tilde{y}} - Y_{\tilde{x}} Y_{\tilde{y}} = 0, \quad (26) \end{aligned}$$

where $T_t \equiv \partial_t T(t, \tilde{x}, \tilde{y})$, etc.

Isothermal coordinates can always be found for surfaces of revolution, by using the meridian and parallel parametrization. To see it, use the following reparametrization of (13):

$$x(\tilde{R}, v) = \tilde{R} \cos v, \quad y(\tilde{R}, v) = \tilde{R} \sin v, \quad z(\tilde{R}) = f(\tilde{R}), \quad (27)$$

so that $dl^2 \equiv dx^2 + dy^2 + dz^2 = (1 + f'^2(\tilde{R}))d\tilde{R}^2 + \tilde{R}^2 dv^2$, and then use $\tilde{u} \equiv \int \sqrt{1 + f'^2(\tilde{R})}/\tilde{R} d\tilde{R}$, which gives $dl^2 = \tilde{R}^2(\tilde{u})(d\tilde{u}^2 + dv^2)$ with $\tilde{R}(\tilde{u})$ obtained by inverting the definition of \tilde{u} . Note that $\tilde{u}(u)$, and $\tilde{R}(\tilde{u}(u)) = R(u)$. This means that for surfaces of revolution⁵

$$\varphi(\tilde{x}, \tilde{y}) = \tilde{R}(\tilde{u}). \quad (28)$$

Thus focusing on the surfaces of revolution (and of constant \mathcal{K}), we are moving in the right direction, but this does not guarantee that we can always succeed to find the coordinates Q^μ this way.

For the sphere, it is easy to find the isothermal coordinates

$$\tilde{x} = v, \quad \tilde{y} = \ln \left(1 + \frac{2}{\cot(u/2r) - 1} \right), \quad (29)$$

for which⁶

$$dl^2 = du^2 + r^2 \cos^2 \frac{u}{r} dv^2 = \frac{r^2}{\cosh^2 \tilde{y}} (d\tilde{x}^2 + d\tilde{y}^2); \quad (30)$$

⁵For a generic surface, i.e., not a surface of revolution, this is not the case. If we could have the general procedure to go from a parametrization of the surface where the visualization is easy [the canonical parametrization (13) being one example], to the isothermal coordinates that give the conformal factor φ^2 , we would immediately know the profiles that graphene should have in order to correspond to important algebraic structures, such as the Virasoro algebras (for $\mathcal{K} = 0$) and the Liouville structures (for $\mathcal{K} \neq 0$), which naturally emerge here in terms of the conformal factor φ^2 ; see [8]. Among the latter, for instance, particularly rich are the vortex solutions of the Liouville equation found in [50].

⁶To see the full match with (28) let us consider, for simplicity, a unit sphere, $r = 1$, centered at the origin, and let us use the standard parametrization $x = \sin\theta \cos\chi$, $y = \sin\theta \sin\chi$, $z = \cos\theta$. For this, $\tilde{R}(\tilde{u}(\theta)) = \sin\theta$. Hence, from $x^2 + y^2 + z^2 \equiv \tilde{R}^2 + z^2 = 1$, one gets $z = \sqrt{1 - \tilde{R}^2} = f(\tilde{R}) = \cos\theta$. Applying the procedure above, $\tilde{u} = \int 1/\tilde{R} \sqrt{1 + \tilde{R}^2/(1 - \tilde{R}^2)} = \ln \tan(\theta/2)$, or $\theta = 2 \arctan e^{\tilde{u}}$, which gives $\tilde{R} = \sin\theta = 1/\cosh \tilde{u}$ (that is also a nice formula to relate trigonometric and hyperbolic functions without resorting to complex numbers). Then, defining $\tilde{u} = \tilde{y}$ and $v = \tilde{x}$, one gets the line element (30).

hence⁷ $\varphi^2(\tilde{y}) = r^2/\cosh^2 \tilde{y} = r^2 \cos^2 \frac{u}{r} = \varphi^2(u)$. One can also check that the Liouville equation is satisfied.⁸

Later we shall show that there is no horizon in this case, and hence no Hawking phenomenon takes place. This makes the sphere a case less apt for the emergence of unmistakable signatures of QFT in curved spacetime. All of this makes us focus on the cases of constant negative curvature. Before moving to those cases, let us add here that the formulas for the sphere we have reobtained above are well known; see, e.g., [13]. The reason for showing them here is that they illustrate, in a very familiar case, that having found the isothermal coordinates, (\tilde{x}, \tilde{y}) , their link with Euclidean coordinates (those measurable in a lab) needs to be made explicit. The expressions (29) are one example. This issue, for the sphere, has been solved over the centuries by map makers.⁹ Less usual is to find solutions for the surfaces of our interest, of which we shall discuss next.

A. Surfaces with $\mathcal{K} = \text{constant} < 0$

For these surfaces, the spatial part of the metric of graphene can be written, in isothermal coordinates, as

$$dl^2 = \frac{r^2}{\tilde{y}^2} (d\tilde{x}^2 + d\tilde{y}^2), \quad (31)$$

where \tilde{x}, \tilde{y} are the *abstract coordinates* of the Lobachevsky geometry in the upper half-plane ($\tilde{y} > 0$) model. One then immediately realizes that our goal is nearer. Indeed, the full line element is

$$ds_{\text{graphene}}^2 = \frac{r^2}{\tilde{y}^2} \left[\frac{\tilde{y}^2}{r^2} dt^2 - d\tilde{x}^2 - d\tilde{y}^2 \right], \quad (32)$$

where the line element in square brackets is *flat*. This apparently solves our problem: the coordinates Q^μ appear to be $(t, \tilde{x}, \tilde{y})$, as there we shall always have the explicit conformal factor $\varphi^2(\tilde{y}) = r^2/\tilde{y}^2$ to implement the Weyl symmetry. Furthermore, the line element in square brackets is of the Rindler kind (see, e.g., [21]); hence it is pointing toward a Unruh kind of effect available for all surfaces of this family. Nonetheless, although this is an important indication, we cannot conclude yet for any Unruh-Hawking kind of effect, hidden in the line element (32), until we make contact with what can be seen in a real laboratory (not in a ‘‘Lobachevsky laboratory,’’ so to speak).

⁷We used here that, when $u = 2r \operatorname{arccot}(\frac{2}{e^{\tilde{y}-1}} + 1)$, $\cos(u/r) = 1/\cosh \tilde{y}$.

⁸In the isothermal coordinates (\tilde{x}, \tilde{y}) , the Liouville equation is $\mathcal{K} = -\frac{1}{2\varphi} (\ln \varphi)''$. With $\varphi = r^2/\cosh^2 \tilde{y}$, one immediately finds the result $\mathcal{K} = 1/r^2$.

⁹For instance, the Mercator projection is precisely the $\tilde{x} = v$, $\tilde{y} = \ln \tan(\theta/2)$ discussed in the footnote.

As said, we need to refer to coordinates measurable in the Euclidean space \mathbf{R}^3 of the laboratory; hence we have to specify \tilde{x} and \tilde{y} in terms of coordinates measurable using the Euclidean distance (embedding), say the (u, v) coordinates. If we are lucky, the result will be globally valid already in the frame (t, u, v) . Otherwise, we need to change coordinates again, and this means, in general, that we have to abandon the lab time t .

Let us recall here the basic facts of Lobachevsky geometry; for more details see [28]. In particular, we focus on the subtle points of embedding this geometry into the Euclidean space. The upper-half plane, $\{(\tilde{x}, \tilde{y}) | \tilde{y} > 0\}$, equipped with the metric (31), represents Lobachevsky geometry, both locally and globally. All other realizations (the Poincarè disk and the Minkowski model, being the other most used two) are related to it; see, e.g., [28]. The geodesics for (31) are semicircles, starting and ending on the “absolute,” the boundary of the space, namely the \tilde{x} axis. Every surface of constant negative Gaussian curvature is locally isometric to the upper-half plane with metric (31). This means that we can work with this metric but have to remember its abstract nature. If we explicitly have \tilde{x} or \tilde{y} in a formula, when it is time to measure, we have to express them in terms of Euclidean coordinates. Since, from (32) we already have the explicit conformal factor we wanted, that is r^2/\tilde{y}^2 , we have to focus on the \tilde{y} coordinate. Indeed, we might run into troubles when we write the specific \tilde{y} for the given surface. The reason is that non-Euclidean geometry objects are “intruders” in a Euclidean world.

In the literature, when a spacetime of negative curvature in n dimensions (such as the anti-de Sitter, AdS_n), is considered, the embedding is done in the unphysical higher dimensional flat spacetime with signature, e.g., $(+, -, \dots, -, +)$; see, e.g., [16,17]. This could be described, for instance, by a spacetime with all real coordinates, say $t, x, \dots, y \in \mathbf{R}$, but one spatial coordinate that necessarily is imaginary, say $z = i\zeta, \zeta \in \mathbf{R}$. Here, as we want to realize such spacetimes in a real lab, we shall always embed in the physical spacetime $(+, -, -, -)$, i.e., $t, x, y, z \in \mathbf{R}$. On this we shall elaborate more in the following section.

1. Beltrami pseudosphere: Global predictability in the simplest frame

Let us now see how all the above comes about in practice. We focus on the Beltrami pseudosphere. If we take \tilde{y} in (31) such that

$$\ln \tilde{y} = -(u/r + \ln c), \quad (33)$$

then $d\tilde{y}/\tilde{y} = -du/r$, or $du^2 = (r^2/\tilde{y}^2)d\tilde{y}^2$, so the choice

$$\tilde{x} = \frac{v}{r}, \quad \tilde{y} = \frac{1}{c} e^{-u/r}, \quad (34)$$

in (31) gives the line element of the Beltrami pseudosphere

$$dl^2 = du^2 + c^2 e^{2u/r} dv^2. \quad (35)$$

The equations above connect “unmeasurable” objects, \tilde{x}, \tilde{y} , to measurable ones, u and v , the meridian and the parallel coordinates. Up to now, it does not appear to be such a different situation as the one depicted before for the sphere; see (29). In fact, the big difference is that we can only represent a tiny sector of the Lobachevsky plane into \mathbf{R}^3 , namely what is called a “horocyclic sector”; see Fig. 2. This fact is governed by a deep result of Hilbert that says [15,51]: *There exists no analytic complete surface of constant negative Gaussian curvature in the Euclidean three-dimensional space.* By “complete” it is meant a surface that does not exhibit singularities.

The horocycles, in the upper-half-plane model, are curves whose normals all converge asymptotically. Since the geodesics here are the following: (a) semicircles starting and ending on the \tilde{x} axis, and (b) half-lines starting on the \tilde{x} axis (that are just the limiting case of the former case), we have two kinds of horocycles—full circles tangent to the absolute for (a), and lines parallel to the absolute for (b). Sectors of horocycles are, essentially, the Lobachevsky version of stripes; see Fig. 2 and [28]. Once one realizes that it is impossible to represent the whole of the Lobachevsky geometry on a real surface, the next most natural thing to try is to see whether, at least, a stripe can be represented. This is, essentially, what Beltrami discovered. The details about the actual construction of this pseudosphere from the Lobachevsky plane are in Fig. 2, and the details on the parametric expression in \mathbf{R}^3 are in Fig. 3.

One important point for us is that, by looking at the expressions (34), we see that \tilde{y} is a smooth, well-behaved, single-valued function, and, to take a full turn on a parallel, $\tilde{x} \rightarrow \tilde{x} + 2\pi/r$, has no effects on \tilde{y} . For this coordinate, the only thing we need to care about is that the surface ends abruptly at $\tilde{y}_{\min} = 1/r$, corresponding to the maximal circle, $R(u = r \ln \frac{r}{c}) = r$. This maximal circle is what we call the “Hilbert horizon,” to recall that it is an effect of the Hilbert theorem on the embedding in \mathbf{R}^3 , and that there the Beltrami spacetime ends. This notion of horizon will be put in contact with that of a proper event horizon in the following. Let us notice here that not always are the singular boundaries one has to expect for a generic surface of this family so clean. In general, they could be a discrete set of points, open/closed curves, self-intersecting open/closed curves, or a combination of these. This depends on the particular embedding, which can be quite involved (see, e.g., [48]). Thus, not always is it such an easy task to identify a Hilbert horizon.

For the Beltrami surface, all the geometrical problems are solved at once: we have an explicit conformal factor that, through the realization (34), is well defined all over the nonsingular part of the surface (and the singular

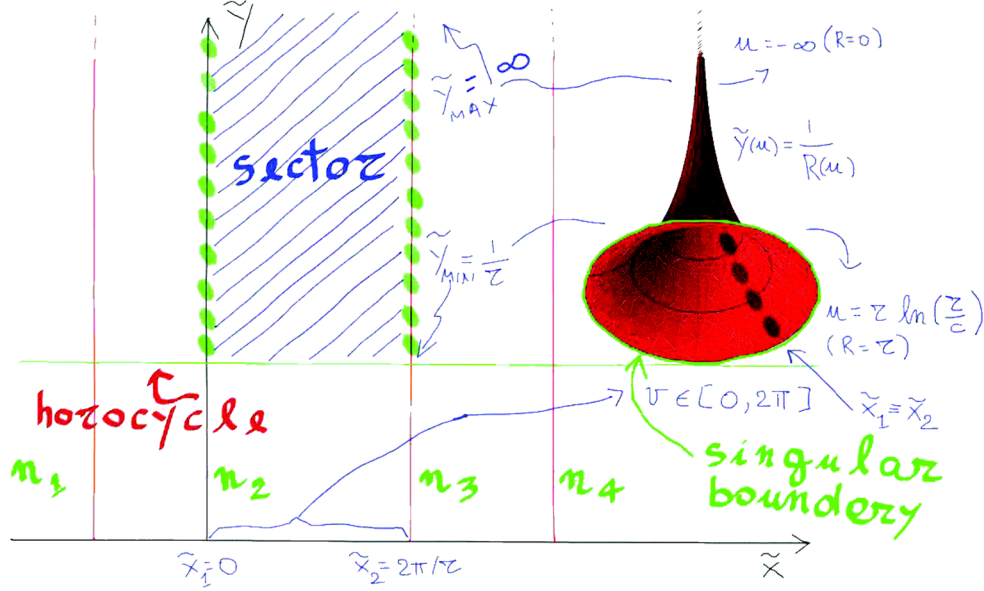


FIG. 2 (color online). Here we build explicitly the Beltrami pseudosphere from the horocyclic sector indicated in the figure. The boundaries to be identified are the indicated portions of the normals n_2 and n_3 . The point at infinity here is $\tilde{y}_{\max} = \infty$, and it would be the same for any choice of horocycles of this kind. The other end of the surface, corresponding to $\tilde{y}_{\min} = 1/r$, is a singular boundary, as predicted by the Hilbert theorem. The range of the meridian coordinate is, of course, $v \in [0, 2\pi]$, while the range of the parallel coordinate u is obtained through the equation $\tilde{y}(u) = 1/R(u)$, and $R(u) = ce^{u/r}$; see Eqs. (34).

boundary is a circle), already in the frame of reference $q^\mu = (t, u, v)$, where the time is exactly the lab time. For this surface, then, using the Weyl symmetry, we can extract sensible predictions based on the line element in square brackets in (32). The latter line element, for this

pseudosphere, coincides with a proper Rindler line element, modulo some differences; see [9] and the next section. Based on this fact, the event horizon we evoked in [9] for the Beltrami spacetime is of the Rindler type, reached at future null infinity, i.e., time-wise. Nonetheless, later we shall show that, by properly taking into account the physical relevance of the parameter c , the Rindler horizon can also be reached space-wise, and it coincides with the Hilbert horizon.

We shall discuss all these points in the next section. Before that, let us have a closer look at the other surfaces of this family.

2. Hyperbolic and elliptic pseudospheres, and other pseudospherical surfaces

For the hyperbolic pseudosphere, we need to solve

$$dl^2 = \frac{r^2}{\tilde{y}^2} (d\tilde{x}^2 + d\tilde{y}^2) \equiv du^2 + c^2 \cosh^2 \frac{u}{r} dv^2, \quad (36)$$

which gives

$$\tilde{x} = e^{cv/r} \tanh(u/r), \quad \tilde{y} = e^{cv/r} \frac{1}{\cosh(u/r)}. \quad (37)$$

From here it is evident that, in the frame $q^\mu = (t, u, v)$, contrary to the Beltrami pseudosphere, we do not have a globally predictive power. The conformal factor, r^2/\tilde{y}^2 , at a fixed value of the meridian, \tilde{u} , will jump out of $e^{-4\pi c/r} r^2 \cosh^2(\tilde{u}/r)$ after a complete turn from 0 to 2π ; see Fig. 4.

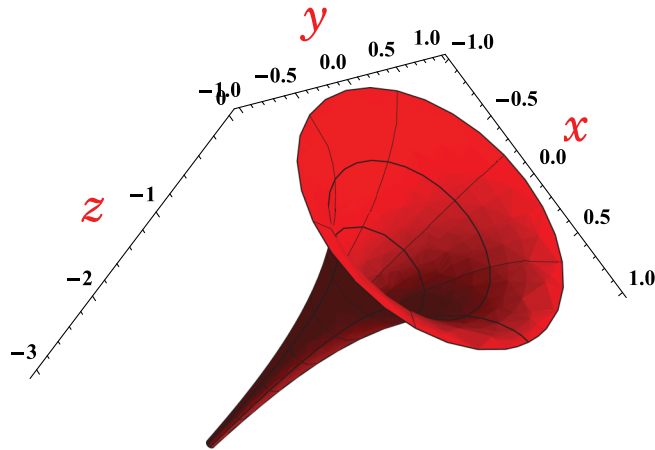


FIG. 3 (color online). The Beltrami pseudosphere is an infinite surface. It is identified by $R(u) = ce^{u/r}$, with c any positive real constant, and $r = \sqrt{-K}$. We have that $R(u) \in [0, r]$ as $u \in [-\infty, r \ln(r/c)]$. The \mathbf{R}^3 coordinates (embedding) are $x(u, v) = ce^{u/r} \cos v$, $y(u, v) = ce^{u/r} \sin v$, $z(u) = r(\sqrt{1 - (c^2/r^2)e^{2u/r}} - \operatorname{arctanh} \sqrt{1 - (c^2/r^2)e^{2u/r}})$. The surface is not defined for $R > r$ [$z(u)$ becomes imaginary], and this fixes the range of u , the singular boundary being the circle $R = r$ at $u = r \ln(r/c)$. The range of v is $[0, 2\pi]$. In the plot $r = 1 = c$ and $u \in [-3.37, 0]$, $v \in [0, 2\pi]$.

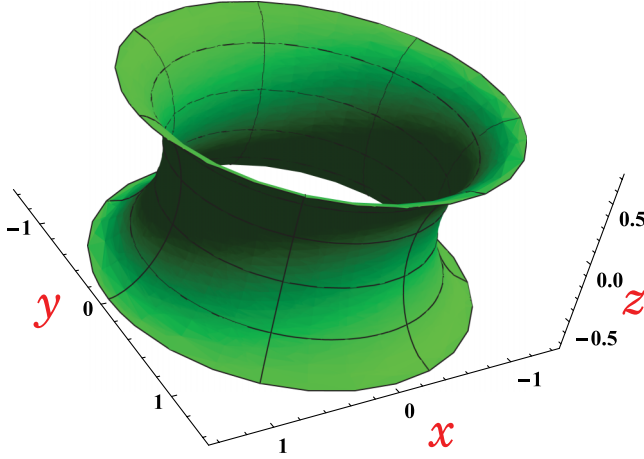


FIG. 4 (color online). The hyperbolic pseudosphere is, in general, a finite surface. It is identified by $R(u) = c \cosh(u/r)$, with c any positive real constant, and $r = \sqrt{-\mathcal{K}}$. The range of R is $R \in [c, \sqrt{r^2 + c^2}]$. According to the general results, the \mathbf{R}^3 coordinates are [13] $x(u, v) = c \cosh(u/r) \cos v$, $y(u, v) = c \cosh(u/r) \sin v$, $z(u) = -iE \int [i(u/r), -(c/r)^2]$, where the last symbol is the elliptic integral. In the plot $r = 1 = c$, and $u \in [-\text{arc cosh } \sqrt{2}, +\text{arc cosh } \sqrt{2}]$, $v \in [0, 2\pi]$ and the range of u is dictated by the condition that $z \in \mathbf{R}$ in terms of the elliptic integral. The singular boundaries in this case are the two extremal circles $R = \sqrt{r^2 + c^2} = \sqrt{2}$, where $u = \pm \text{arc cosh } \sqrt{2}$.

This does not mean that we cannot do anything with this pseudosphere. We have three roads to follow: (a) we make *locally* valid predictions in the coordinates q^μ ; (b) we find a new coordinate system, where Weyl symmetry gives a globally well defined conformal factor, but points to a curved spacetime, rather than to a flat spacetime; (c) we find coordinates Q^μ for which we have both things at work, Weyl symmetry linking this spacetime to the flat one, *and* a global predictive conformal factor. Later we shall use a mixture of the options (a) and (b), but let us illustrate the strategy (c) at work for yet another pseudosphere, the elliptic.

To solve

$$d\ell^2 = \frac{r^2}{\tilde{y}^2} (d\tilde{x}^2 + d\tilde{y}^2) \equiv du^2 + c^2 \sinh^2 \frac{u}{r} dv^2 \quad (38)$$

is cumbersome, because the most natural model for this pseudosphere is the Poincaré disk model, rather than the upper half-plane. The results for $\tilde{x}(u, v)$ and $\tilde{y}(u, v)$ are too messy to show here, and, in any case, as for the previous pseudosphere, they also exhibit multivaluedness of the \tilde{y} coordinate. On the other hand, by solving (a system related to) (25) and (26), we find that the following coordinates:

$$\begin{aligned} T &= re^{t/r} \cosh\left(\frac{u}{r}\right), & X &= re^{t/r} \sinh\left(\frac{u}{r}\right) \cos\left(c\frac{v}{r}\right), \\ Y &= re^{t/r} \sinh\left(\frac{u}{r}\right) \sin\left(c\frac{v}{r}\right), \end{aligned} \quad (39)$$

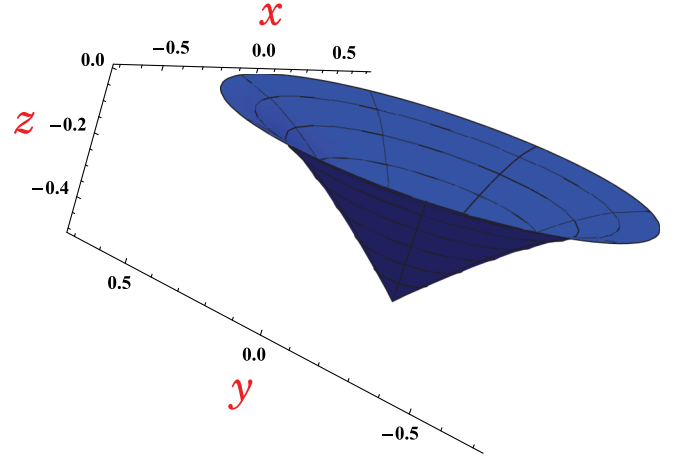


FIG. 5 (color online). The elliptic pseudosphere is, in general, a finite surface. It is identified by $R(u) = c \sinh(u/r)$, with $c < r$, and $r = \sqrt{-\mathcal{K}}$. A good parametrization of the constants, due to Ricci [13], is $c = r \sin \vartheta$ (note that $c = r$ is a degenerate case, giving a circle), and hence the range of R is $[0, r \cos \vartheta]$. The \mathbf{R}^3 coordinates can be obtained from the general results, $x(u, v) = r \sin \vartheta \sinh(u/r) \cos v$, $y(u, v) = r \sin \vartheta \sinh(u/r) \sin v$, with $z(u)$ given in terms of elliptic integrals through $z = \pm \int \sqrt{1 - R'^2(u)}$. In the plot $r = 1$, $\vartheta = \pi/4$ and $u \in [0, 2]$, $v \in [0, 2\pi]$, and the range of u is dictated by the condition that $z \in \mathbf{R}$. The singular boundaries in this case are the point $R = 0$, corresponding to $u = 0$, and the maximal circle of radius $R = r \cos \vartheta$, corresponding to u_{\max} .

with $0 < c < r$, give a perfectly well defined conformal factor ϕ for the $(2+1)$ -dimensional metric [see last expression in (24)]

$$\phi^2 = r^2 / (T^2 - X^2 - Y^2) = e^{-2t/r}. \quad (40)$$

One can surely imagine a physical situation where those coordinates make physical sense, but we shall not follow this road because its experimental realization does not look easy. In fact, there is the same alternative road as for the previous pseudosphere, involving another curved spacetime and the Beltrami spacetime, that gives sensible results

There are many examples in the literature of the other pseudospherical surfaces, infinite in number; see, e.g. [15,48]. From there, one immediately realizes that the tasks we have accomplished in such a clean way with the Beltrami spacetime are, in general, much more difficult.

Nonetheless, all those surfaces are described by the line element (31), and hence the general result of geometry recalled earlier comes in hand [13]: *The line element of any surface of constant negative Gaussian curvature, not necessarily a surface of revolution, is reducible to the line element of the Beltrami or the hyperbolic or else the elliptic pseudospheres*, given here by (14) with (18), (19), and (20), respectively. This is achieved by having the geodesics system of the given surface coincide (though a mapping)

with the geodesics system of the particular pseudosphere [13]. To this well-known result that points toward three surfaces only, we want to add the following considerations that merge the three into one: the Beltrami. This shows that to consider the Beltrami means to consider, at least locally, all the surfaces of the family.

In general, the three pseudospheres (18)–(20) differ importantly from each other, and the previous theorem is one example of this. Indeed, besides the differences just discussed about their natural coordinate systems in a $(2+1)$ -dimensional spacetime, the Beltrami surface is infinite, while the other two are not. Furthermore, the Beltrami surface has one singular boundary only, at $R = r$, while the other two pseudospheres have two singular boundaries: the hyperbolic pseudosphere when

$R = \sqrt{r^2 + c^2}$, the elliptic at $R = 0$ and at $R = r \cos \vartheta$. Nonetheless, *in the limit of very small c/r* , the three surfaces have very similar behavior. This can be seen by the inspection of the expressions in (18)–(23) and is depicted in the plots of Fig. 6 that have to be compared with the plot in Fig. 3. In the limit $c/r \rightarrow 0$, the range of u is infinite for all, the range of R is $[0, r]$ for all, and in the positive u sector, they all approach the same form [see (18)–(20)]

$$R(u) \sim ce^{u/r} \in [0, r] \quad \text{when } u \in [0, +\infty] \quad (41)$$

(we shall be more precise in the following section about the actual limits of the range of u that crucially depend upon the physics of the application to graphene).

With this in mind, we shall mostly focus on the Beltrami spacetime, as the results are the cleanest there and can serve as a guide for the other (infinite number of) cases too. On the other hand, the mappings among the three different pseudospheres will reinforce the conclusions of [9] about the existence of an event horizon on the Beltrami spacetime, as we shall show next.

V. RELATIVITY ISSUES: THE HORIZON

There are various kinds of horizon in general relativity, sometimes differing for very subtle reasons; see, e.g., [52–54]. We do not yet have at our disposal the gravity/geometrical theory that describes the dynamics of the elastic membrane of graphene (the effective description of the dynamics of the σ bonds), and thus we cannot yet embark in such subtle distinctions. One distinction we can attempt to make, though, is between the singular boundary of the surfaces of constant negative curvature that we call the Hilbert horizon (when it is possible to identify it as the end of the spacetime, as, e.g., the circle $R = r$ of the Beltrami surface) and a standard event horizon (e.g., the horizon of Rindler spacetime). These two types of horizon, for a generic surface of constant negative Gaussian curvature, are in principle different. But, below, we shall show that, in the case of a Beltrami spacetime, in the physically appropriate limit of small c/r , the two horizons coincide within very reasonable experimental errors. Furthermore, in that limit, the same Hilbert horizon, $R = r$, is (Weyl) related to three standard event horizons: the Rindler kind, the cosmological kind, and the black-hole kind (although, in this latter case, in the limit of vanishing black-hole mass). To the latter two cases are dedicated Appendix A and Appendix B, respectively.

Let us start by finding some general results, valid for the infinite number of cases of constant negative Gaussian curvature. We need to consider the line element (32)

$$ds_{\text{graphene}}^2 = \frac{r^2}{\tilde{y}^2} \left[\frac{\tilde{y}^2}{r^2} dt^2 - d\tilde{y}^2 - d\tilde{x}^2 \right],$$

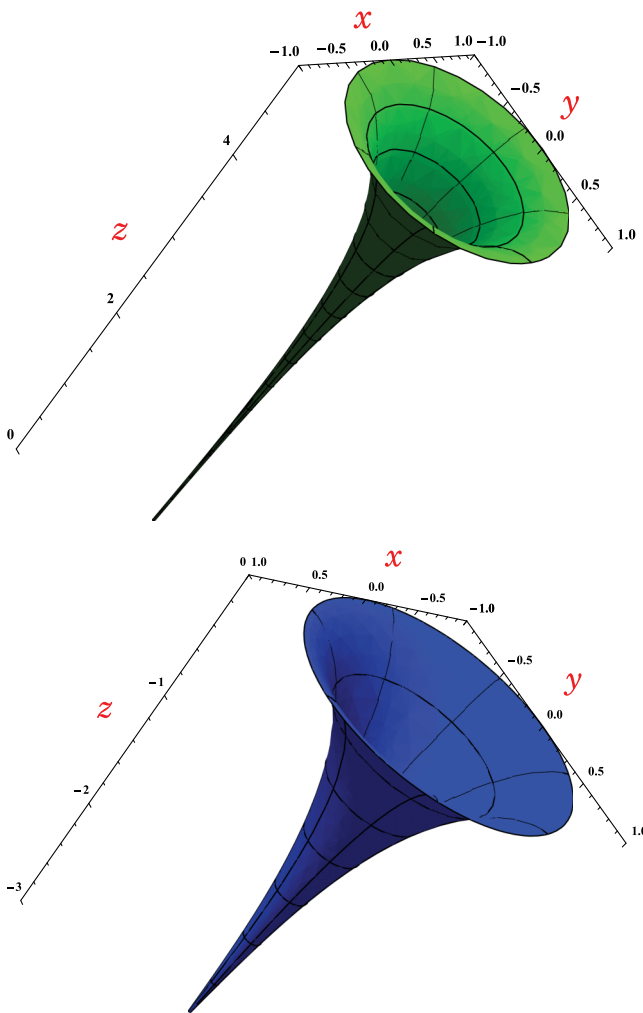


FIG. 6 (color online). In these two examples, one-half of the hyperbolic pseudosphere (above) and the full elliptic pseudosphere (below), for small values of c/r . It is evident that both cases are similar to the Beltrami case of Fig. 3, as discussed in the text. For the half of the hyperbolic pseudosphere, the plot here is for $r = 1$ and $c = 0.01$. For the elliptic pseudosphere, the plot here is for $r = 1$, and $\vartheta = \pi/50 \simeq 0.06 \simeq c$.

and either study separately the Rindler-like spacetime and the conformal factor or study directly the full line element $dt^2 - (r/\tilde{y})^2(d\tilde{x}^2 + d\tilde{y}^2)$ (the results are, of course, the same). The null geodesics¹⁰ of both spacetimes are of this form

$$\tilde{x}(t) = \text{const} \quad \text{and} \quad \tilde{y}(t) = \tilde{y}_0 e^{\pm v_F t/r}, \quad (42)$$

where we have, momentarily, reintroduced v_F (our “speed of light”), and $+$ ($-$) is for the outgoing (ingoing) trajectories (for antiparticles signs swap). The actual *Euclidean length* can be obtained only when the Lobachevsky coordinate \tilde{y} has been expressed in terms of Euclidean measurable spatial coordinates, hence when the surface has actually been specified. On the other hand, to make general statements we look at the *Lobachevsky length*. Equations (42) identify a straight line of the degenerate type in the Lobachevsky plane, and the Lobachevsky distance between two points is

$$\begin{aligned} d(\tilde{y}(t_2), \tilde{y}(t_1)) &= \text{arccosh} \left(1 + \frac{(\tilde{y}(t_2) - \tilde{y}(t_1))^2}{2\tilde{y}(t_2)\tilde{y}(t_1)} \right) \\ &= \frac{v_F}{r} |t_2 - t_1|, \end{aligned} \quad (43)$$

with $\tilde{y}(t)$ in (42).

The above discussion means that the pseudoparticles, on a generic graphene surface of constant negative curvature, see

$$\tilde{y} = 0$$

as an event horizon: (a) the metric elements are singular there, and (b) it can only be reached asymptotically at future null infinity (it can never be crossed). Thus, one thing we learn from the above discussion is that, even when only spatial curvature is present, and all metric variables are time independent, an event horizon is indeed possible. The issue here is, does the curve¹¹ $\tilde{y} = 0$ belong to the spacetime?

First of all, by the very definition of the Lobachevsky plane, strictly speaking, $\tilde{y} = 0$ is excluded from the manifold. It is the absolute¹² of the upper-half plane model, and hence all considerations about having it into the spacetime have to be about limiting processes. Nonetheless, this situation is common to standard event horizons, when the coordinates are such that the inner region beyond the

¹⁰Our considerations refer to the pseudoparticles of graphene that are massless (Dirac) excitations.

¹¹By “curve” we mean the set of points in the *Euclidean coordinates* that are a solution of $\tilde{y} = 0$ for the given surface/spacetime. Strictly speaking, there is no such solution.

¹²This makes clear that the choice of other models for Lobachevsky geometry would make no difference in this important respect.

horizon is out of reach. A well-known example is the event horizon for a spherically symmetric black hole in the Schwarzschild coordinates.

In this latter case, the coordinates can be changed, for instance to the Eddington-Finkelstein coordinates, and the singular behaviors of infinite geodesic distance and infinite metric elements (that we just used to identify $\tilde{y} = 0$ as an event horizon) go away, changing the properties of a horizon into those of a one-way membrane [or “one-brane,” for this $(2+1)$ d case]: ingoing particles can cross the horizon, but outgoing cannot.

In our case there is no equivalent of the Eddington-Finkelstein coordinates. The horizon can never be crossed, no matter the coordinates. The coordinates, though, are crucial, because only when we specify the surface (i.e., when we find the Euclidean coordinates to realize a portion of the Lobachevsky plane in the \mathbf{R}^3 of the laboratory) we can face the questions on whether (i) the Hilbert horizon is a well defined object, and (ii) it is close enough to the event horizon.

In all cases, the Hilbert horizon is located where its smaller \tilde{y} coordinate, say it is \tilde{y}_{Hh} , is strictly bigger than that of the event horizon, $\tilde{y}_{Hh} > 0$. In general, we cannot say whether the Hilbert horizon is close to or far from the event horizon. Indeed, this depends on the fine details of the given surface. Each of the infinite surfaces has its own structure of singularities. It might well be that there is more than one Hilbert horizon (see, e.g., the hyperbolic pseudosphere in Fig. 4), or it might even happen that it is not easy to identify a reasonable Hilbert horizon, i.e., a curve where the spacetime ends. What we shall see now is the following: (a) for the Beltrami spacetime the Hilbert horizon is a clean object and, in the limit of small c/r , Weyl related to a very reasonable *Rindler event horizon*; (b) for the elliptic pseudosphere the Hilbert horizon is a clean object and, in the same limit, Weyl related to a reasonable *cosmological (de Sitter) event horizon*; (c) for the hyperbolic pseudosphere, the Hilbert horizon is a clean object and in the same limit, Weyl related to a *black hole (BTZ) event horizon*, although in the limiting case of vanishing mass. In the last two cases, as already shown, in the limit of small c/r , the spacetime tends to the Beltrami spacetime¹³; hence the surface and the Hilbert horizon, in all cases, are the same ones.

These results will, on the one side, reinforce and improve the results of [9] on the Rindler horizon for the Beltrami spacetime. On the other side, since all surfaces of constant negative Gaussian curvature are locally isometric to the Beltrami pseudosphere, these results also are an empirical proof that when on one surface of the family the conditions

¹³There are, though, some global differences: the elliptic pseudosphere is singular also at the tip of the tail ($R = 0$), while the hyperbolic pseudosphere tends to two Beltramis joined at $R = 0$ (see Fig. 10), hence evoking a wormhole-type of spacetime with two Hilbert/event horizons.

for a horizon are reached, and the results about thermal Green functions found for the Beltrami spacetime [9] can be used, although their validity might be confined to a small neighbor. On this latter point we shall come back later. We want to prove now the previous statements about the Rindler horizon (Appendixes A and B are dedicated to the de Sitter and BTZ horizons, respectively).

A. The Rindler-like horizon of Beltrami spacetime

By using the expressions (34) in (32), and by introducing the correct dimensionality for the coordinates, so that the conformal factor is dimensionless,¹⁴ the line element of the Beltrami spacetime is

$$ds_B^2 = \frac{c^2}{r^2} e^{2u/r} \left[\frac{r^2}{c^2} e^{-2u/r} (dt^2 - du^2) - r^2 dv^2 \right] \equiv \varphi^2(u) ds_R^2, \quad (44)$$

with $\varphi(u) \equiv c/re^{u/r}$, and

$$ds_R^2 \equiv \frac{r^2}{c^2} e^{-2u/r} (dt^2 - du^2) - r^2 dv^2, \quad (45)$$

where the subscript “R” stands for Rindler, and from now on we take

$$c < r, \quad (46)$$

so that $\ln(r/c)$ is always greater than zero.

Just like in the standard case, the line element ds_R^2 in (45) describes both the left and the right Rindler wedges. Indeed,

$$\eta \equiv \frac{r}{c} t \in [-\infty, +\infty] \quad \text{and} \quad v \in [0, 2\pi] \quad (47)$$

but, for $a \equiv c/r^2 > 0$

¹⁴This amounts to introducing Lobachevsky coordinates of dimension of (length) $\tilde{x} \rightarrow r^2 \tilde{x}$ and $\tilde{y} \rightarrow r^2 \tilde{y}$. Having done that, though, there is a more straightforward choice than (44) to have a dimensionless conformal factor multiplying a line element of the right dimensions of (length)², namely $ds_B^2 = e^{2u/r} [e^{-2u/r} (dt^2 - du^2) - c^2 dv^2]$. For the latter choice, the conformal factor, evaluated at the Hilbert horizon, diverges for $c \rightarrow 0$, $\varphi(u = r \ln(r/c)) = r/c \rightarrow \infty$. This is as it must be for a proper event horizon, and it can also be taken as a piece of evidence of the coincidence of Hilbert and event horizons in the limit for $c \rightarrow 0$. Nonetheless, the metric elements (see the angular part $c^2 dv^2$) make no sense in the limit $c \rightarrow 0$, no matter whether one is at the horizon. Thus we prefer the choice (44), along with a redefinition of the coordinates [$t \rightarrow (r/c)t$, $u \rightarrow (r/c)u$, see later], so that the divergent behavior in the $c \rightarrow 0$ limit is passed on from the metric elements to the range of the coordinates. The choice (44) gives a conformal factor that, at the horizon, is always finite, $\varphi(u = r \ln(r/c)) = 1$. No matter the choice, though, the indication of how close the Hilbert horizon of the Beltrami spacetime is to the event horizon of a Rindler spacetime is always given by how small is c/r , as will be clear from the following.

$$\xi \equiv -\frac{r}{c} u \in [-(r^2/c) \ln(r/c), +\infty], \quad (48)$$

while, for $a \equiv -c/r^2 < 0$

$$\xi \equiv \frac{r}{c} u \in [-\infty, +(r^2/c) \ln(r/c)], \quad (49)$$

so that

$$\tilde{y} = \frac{1}{c} e^{-u/r} = \begin{cases} +\frac{1}{ar^2} e^{a\xi} > 0 & \text{right wedge,} \\ \text{or} & \\ -\frac{1}{ar^2} e^{a\xi} > 0 & \text{left wedge.} \end{cases} \quad (50)$$

Here a is the value of the proper acceleration $\alpha(\xi)$ evaluated at the origin of the Rindler spatial coordinate, $\xi = 0$, and the proper acceleration is defined in accordance to the line element

$$ds_R^2 = e^{2a\xi} (d\eta^2 - d\xi^2) - r^2 dv^2, \quad (51)$$

so that $e^{-a\xi}$ is the appropriate Tolman factor

$$\alpha(\xi) = ae^{-a\xi}. \quad (52)$$

Now we focus on the line element (51), knowing that this spacetime differs from a standard Rindler spacetime only with respect to the range of the ξ coordinate (and for the fact that the “speed of light” here is v_F ; on this see the next section). In the standard Rindler spacetime, the event horizon is identified *space-wise* by

$$\xi_{Eh} = -\infty \text{ right wedge} \quad \text{and} \quad \xi_{Eh} = +\infty \text{ left wedge}, \quad (53)$$

and *time-wise* by

$$\eta = +\infty. \quad (54)$$

In [9] we focused only on the latter. Here, in the spirit of the previous general discussion, we want to focus on the former, to see under which conditions the event horizon is within the reach of the Beltrami spacetime, and its relationship to the Hilbert horizon, located at

$$\begin{aligned} \xi_{Hh} &= -\frac{r^2}{c} \ln(r/c) \text{ right wedge} \quad \text{and} \\ \xi_{Hh} &= +\frac{r^2}{c} \ln(r/c) \text{ left wedge.} \end{aligned} \quad (55)$$

Clearly, $\xi_{Hh} \rightarrow \xi_{Eh}$ for $c \rightarrow 0$. Let us now investigate the physics of this limit. For definitiveness, we shall consider *the right wedge* for the rest of this section.

In the standard Rindler case, the inertial observer is the one for which the proper acceleration is zero, i.e.,

$\xi_{\max} = +\infty$. Thus, the range of ξ is dictated by the following two conditions: (i) its minimum corresponds to the event horizon, and there the acceleration reaches its maximum; (ii) its maximum corresponds to the inertial observer ($\alpha = 0$)

$$\xi \in [-\infty, \dots, 0, \dots, +\infty] \Rightarrow \alpha(\xi) \in [+ \infty, \dots, a, \dots, 0], \quad (56)$$

where we included the middle range value, important for us, and wrote the range of $\alpha(\xi)$ so that it corresponds to the range of ξ . An observer at standard Rindler space coordinate ξ is constantly at a distance

$$d(\xi) \equiv 1/\alpha(\xi) - 1/\alpha_{\max} = 1/\alpha(\xi), \quad (57)$$

from the horizon. The inertial observer is infinitely far away, $d(\xi_{\max} = +\infty) = \infty$, and $d(\xi_{Eh} \equiv \xi_{\min} = -\infty) = 0$. For our spacetime, the ranges in (56), for finite $c < r$, become

$$\begin{aligned} \xi \in \left[-\frac{r^2}{c} \ln(r/c), \dots, 0, \dots, +\infty \right] &\Rightarrow \alpha(\xi) \\ &\in [1/r, \dots, a = c/r^2, \dots, 0]. \end{aligned} \quad (58)$$

If we now consider the mathematical limit $c \rightarrow 0$, with r finite, we see two things. First $a \rightarrow 0$; hence it is $\xi = 0$ (corresponding to $\alpha = a \rightarrow 0$), the coordinate corresponding to the inertial observer. Second, the lower bound of the range, corresponding to the Hilbert horizon, is $-(r^2/c) \ln(r/c) \rightarrow -\infty$, and there $\alpha = 1/r$. So, the range of ξ gets halved, and the maximal acceleration is finite and related to the curvature

$$\xi \in [-\infty, 0] \Rightarrow \alpha(\xi) \in [1/r, 0] \quad \text{when } c \rightarrow 0. \quad (59)$$

In the limit $c \rightarrow 0$, $\xi_{Hh} \rightarrow \xi_{Eh}$, and an observer with space coordinate ξ is constantly at a distance

$$d(\xi) = 1/\alpha(\xi) - 1/\alpha_{\max} = 1/\alpha(\xi) - r \quad (60)$$

from the horizon. Thus, the inertial observer is infinitely far away, $d(\xi_{\max} = 0) = \infty$, while $d(\xi_{Hh} \equiv \xi_{\min} = -\infty) = 0$.

It is important to notice that, even in the limit $c \rightarrow 0$, we are not changing the location of the Hilbert horizon in terms of the Lobachevsky coordinate, as this is once and for all given by $\tilde{y}_{Hh} \equiv \tilde{y}(u_{\max} = r \ln(r/c)) = 1/r$. We are changing its location in terms of the coordinate u .

It is crucial to implement the limit $c \rightarrow 0$ *physically*, i.e., to have c small compared to the only physical scale we have used, that is r , and thus, the crucial parameter is c/r , rather than c . In a moment we shall identify the physical and geometrical meaning of c for the graphene membrane, and we shall fix this length. Thus, we shall have that $\xi_{Hh} \rightarrow$

$-\infty = \xi_{Eh}$ only approximately. Furthermore, to make c/r small we have to make r big.

To understand the physical and geometrical role of c for the Beltrami spacetime, one recalls that $R(u) = ce^{u/r}$; hence we see that c fixes the origin of the u coordinate

$$c = R(u = 0), \quad (61)$$

and this explains, from the point of view of the geometry of the pseudosphere, why, when $c \rightarrow 0$, the range of u gets halved: in that limit, the value $R = 0$ is reached already at $u = 0$. On the other side of the range there is r , and

$$r = R(u_{\max} = r \ln(r/c)). \quad (62)$$

Thus the pace at which one reaches the end of the surface, starting from the origin of the Euclidean measurable coordinate u , is fixed by c : the smaller c , the farther away is the end of the surface, i.e., the more u steps are necessary to reach there. In the limit $c \rightarrow 0$ the number of steps is infinite. The most natural choice for c , then, is to link it to the natural pace of the graphene membrane, which is the lattice spacing. Thus, we choose

$$c = \ell. \quad (63)$$

There is also another reason, perhaps clearer, to fix $c = \ell$, that comes from the geometry of the hyperbolic pseudosphere. There, $c = R(u = 0)$ always corresponds to the minimum value of R ; see Fig. 4. Hence, one cannot think of going below $R = \ell$ for the real membrane. Since, as shown, in the limit of small c/r the two surfaces (and the elliptic pseudosphere) become, in a way, the same surface, and that argument can be imported here too.

This choice of c fits very well our requests of small curvatures ($r > \ell$), necessary for the approach based on the action (10) to work.

Of course, even the choice $c = \ell$ is an idealization, and it must serve only as a guide for the real situation. In fact, our approximations on the dynamics of the conductivity electrons of graphene cannot hold down to such small radii of the pseudosphere. For instance, the distance between different sides of the membrane will become too small to ignore out-of-surface interactions, not to mention the distortions in the lattice structure to make a section of radius [11] $R = \ell$. Nonetheless, as can easily be read off from Table I, the approximations within which the Hilbert horizon and the event horizon coincide are so good that even a much larger c would not change our conclusions. That is why we prefer to present the values for the choice $c = \ell$ that can easily be adapted to a realistic engineering of the graphene membrane, rather than the present values for a choice $c = \delta\ell$, with δ a number that, at the present level of experimental and theoretical knowledge on the manipulation of graphene in order to induce different

TABLE I. Quantification of how good it is to approximate the Hilbert horizon of the Beltrami spacetime, $R = r$, with a Rindler event horizon. The closer $\zeta_B \equiv -(\ell/r)^2/\ln(r/\ell)$ is to zero, the better is the approximation. In the table we indicate three values of r , the corresponding values of ζ_B , and we also explicitly indicate the corresponding values of ℓ/r (recall that $\ell \simeq 2 \text{ \AA}$). This latter parameter is also a measure of how close to zero is $\tilde{y}_{Hh} = 1/r$, in units of the lattice spacing ℓ : $1/(r/\ell)$. The values are all approximate.

r	ζ_B	ℓ/r
20 \AA	-4×10^{-3}	0.1
1 \mu m	-5×10^{-9}	2×10^{-4}
1 mm	-3×10^{-15}	2×10^{-7}

shapes and patterns, is simply a number that one has to guess.

Since the event horizon of a Rindler spacetime is at $1/\xi_{Eh} = 0$, a way to quantify how good are our approximations for the Beltrami spacetime is to see how close to zero, in units of ℓ , is $1/\xi_{Hh}$, which is the dimensionless parameter $\zeta_B \equiv -(\ell/r)^2/\ln(r/\ell)$. Some values are shown in Table I.

Notice that the bigger r , the closer is the horizon. This could have been guessed immediately from $\tilde{y}_{Hh} = 1/r$. Nonetheless, we have to measure in terms of the u coordinate, so even a finite and not too small $1/r$ can still give a very good approximation. For instance, already at $r = 20 \text{ \AA}$, that gives a large value 0.1 for ℓ/r ; the error in identifying $R = r$ as the Rindler event horizon is of a more reasonable four parts per 1000. On the other hand, at a more realistic value of $r = 1 \text{ \mu m}$, that error becomes a reassuring five parts per one billion. For experimental detections of Hawking phenomena associated with the existence of this horizon, we need to compromise between a large enough r for a good horizon and a small enough r for a detectable Hawking temperature, $\mathcal{T} \sim 1/r$. As already seen in [9], and will be further addressed later in this paper, r 's in the range of 1 \mu m – 1 mm are good for the latter purpose and are shown in Table I to be good for the former purpose too.

VI. THE QUANTUM VACUA AND THE MEASUREMENTS

Let us now come to the key issue of which quantum vacuum we need to refer to when computing our Green functions. For this section only, with c we indicate the speed of light in vacuum.

The first thing to consider is that this is a very peculiar situation, with two spacetimes of different natures that come into contact. On the one hand, we have the spacetime of the laboratory, which is $(3 + 1)$ dimensional and *non-relativistic in the sense of c as the limiting speed*

$$ds_{\text{lab}}^2 = c^2 dt^2 - dx^2 - dy^2 - dz^2, \quad (64)$$

so, here the 0th component of the position vector is $X^0 \equiv ct$. Nonrelativistic means that the transformations associated with this line element are ‘‘small’’ $\text{SO}(3,1)$ transformations,¹⁵ i.e., for instance, for a boost along the first axis

$$\Lambda_{\text{full}} = \begin{pmatrix} \gamma & -\beta\gamma & 0 & 0 \\ -\beta\gamma & \gamma & 0 & 0 \\ 0 & 0 & 1 & 0 \\ 0 & 0 & 0 & 1 \end{pmatrix} \in \text{SO}(3,1)_c$$

$$\Rightarrow \Lambda_{\text{small}} \simeq \begin{pmatrix} 1 & -\beta & 0 & 0 \\ -\beta & 1 & 0 & 0 \\ 0 & 0 & 1 & 0 \\ 0 & 0 & 0 & 1 \end{pmatrix} \in \text{SO}(3,1)_c^{\text{small}}, \quad (65)$$

where $\beta \equiv v/c$, and $\gamma \equiv (1 - \beta^2)^{-1/2}$, so that, at the $O(\beta^2)$ approximation, the line element (64) is invariant under Λ_{small} , and one sees that

$$ct' = ct - \beta x \Leftrightarrow t' = t + O(\beta^2) \simeq t, \quad (66)$$

$$x' = x - \beta ct = x - vt, \quad (67)$$

the transformations reduce to Galilei's (far right side); hence time is untouched. The notation $\text{SO}(3,1)_c$ is just to remind one that the elements of the group have c , but group-wise the object is the standard $\text{SO}(3,1)$. Similar considerations hold for $\text{SO}(3,1)_c^{\text{small}}$.

We call this spacetime $\mathbf{R}_{c,\text{small}}^{(3,1)}$, where ‘‘small’’ refers to the associated nonrelativistic transformations. This is an abuse of notation, as the spacetime is, once and for all, $\mathbf{R}_c^{(3,1)}$, but this way we emphasize the fact that, at small velocities compared to c , time decouples entirely from space ($t' = t$), and the very same concept of spacetime has no meaning. Thus a nonrelativistic spacetime is not a Euclidean spacetime [that would amount to have $\text{SO}(4)$ as an invariance group, and hence a like-sign signature, e.g., $(+, +, +, +)$], but a spacetime for which the light cone is so far away from the worldlines that the effects of linking together space and time are negligible, and they are effectively separated entities. The ψ electrons of graphene that move at the Fermi speed $v_F \sim c/300$, *when considered from the laboratory frame*, fit this nonrelativistic scenario very well, since for them $O(\beta^2) \sim 10^{-8}$.

On the other hand, we have the effective spacetime of planar graphene, which is $(2 + 1)$ dimensional and *relativistic in the sense of v_F , Fermi velocity, as limiting speed*

¹⁵We do not consider here the translations, an issue that for graphene deserves further study [46].

$$ds_{\text{graphene}}^2 = v_F^2 dt^2 - dx^2 - dy^2; \quad (68)$$

hence, here the 0th component of the position vector is $x^0 \equiv v_F t$. We choose the planar graphene case, as that is the important case for our considerations. This line element is invariant under $\text{SO}(2,1)_{v_F}$, with the same notation as before; hence, for the boost along x , the matrix is

$$\Lambda_{\text{full}} = \begin{pmatrix} \gamma & -\beta\gamma & 0 \\ -\beta\gamma & \gamma & 0 \\ 0 & 0 & 1 \end{pmatrix} \in \text{SO}(2,1)_{v_F}, \quad (69)$$

but now $\beta \equiv v/v_F$. We call this spacetime $\mathbf{R}_{v_F}^{(2,1)}$, with the notation explained earlier.

Thus, the same time label t enters two dramatically different spacetimes

$$X^0 \equiv ct \in \mathbf{R}_{c \text{ small}}^{(3,1)} \quad \text{and} \quad x^0 \equiv v_F t \in \mathbf{R}_{v_F}^{(2,1)}. \quad (70)$$

From the point of view of the ψ electrons of graphene, t enters the variable x^0 , which is the time part of a proper spacetime distance. The same variable t , for the laboratory observer, enters a different variable X^0 and, being part of a line element that transforms under Galilei transformations, does not contribute to a *spacetime* but only to a time distance, as there space and time are decoupled.

This shows that the inner time variable x^0 , although numerically given by v_F times the same parameter of the outside clocks, is intrinsically different from the external time variable X^0 , from a relativistic point of view. Nonetheless, we have to account for the numerous experimental observations of the v_F -relativistic effects of the ψ electrons of graphene. Within the picture illustrated above, the simplest way is to *describe the external observer/lab spacetime as $\mathbf{R}_{v_F}^{(2,1)}$, and this must hold no matter which spacetime is effectively reached by the ψ electrons of graphene, including curved spacetimes.* Notice that, when the spacetime curvature effects occur on graphene (even only of a spatial kind), it makes no sense to insist on identifying the two spacetimes, the inner and the outer. This would imply a curved laboratory spacetime. Evidently, the only issue is with the time variable, as one can easily envisage an observer constrained to be on a two-dimensional spatial slice. The previous discussion shows that indeed the 0th components on the two sides (graphene and lab) have a different interpretation; hence, when the 0th component on the graphene side can be seen, e.g., as related to a Rindler time (see the previous section and [9]), the 0th component on the laboratory is, once and for all, a $(2+1)$ -dimensional v_F -Minkowski time variable.

The role of the third spatial dimension is not completely gone in this picture, so we do reproduce some physics of the extra dimension. Indeed, in all the previous discussions about the embedding, we have considered $\mathbf{R}_{v_F}^{(3,1)}$. In fact, the role of this larger space is seen only in the effects of

embedding the surfaces in spatial \mathbf{R}^3 (Hilbert horizons, dS vs AdS, etc.). Once the surface is obtained, and the peculiarities of the embedding are taken into account in the resultant $(2+1)$ -dimensional curved spacetime, the external observer/lab spacetime is modeled as $\mathbf{R}_{v_F}^{(2,1)}$.

We could use $\mathbf{R}_c^{(3,1)}$, although this choice is less natural for nonrelativistic (in the sense of c) electrons. This choice would evoke quantum gravity scenarios, where indeed universes with different constants of nature are contemplated. Here we would have two such universes, with different “speeds of light,” that get in contact.¹⁶ We shall not proceed this way here and shall use instead the operationally valid *Ansatz* illustrated above.

It is perhaps worth clarifying that this procedure should in no way be taken seriously from a general point of view. For a generic phenomenon, e.g., the dynamics of a classic nonrelativistic marble rolling on the graphene sheet, the graphene surface is just a surface in a nonrelativistic spacetime. What matters to us is that the procedure works well for the case in point of the ψ electrons of our concern. It is only for them that the spacetime of graphene is v_F relativistic, and not for the classic marble. Furthermore, the ψ electrons here, within the limits of the model illustrated in Sec. II, are the quanta of a quantum field. The procedure then is satisfactorily implemented when we prescribe that the structure of the n -point functions is always of the following kind:

$$S^{\text{any}}(q_1, \dots, q_n) \equiv \langle 0_M | \psi(q_1) \cdots \bar{\psi}(q_n) | 0_M \rangle, \quad (71)$$

where $\psi(q)$, with $q^\mu = (v_F t, u, v)$, is the Dirac quantum field associated with *any* graphene surface, while $|0_M\rangle$ is demanded to be always the quantum vacuum for the Dirac field of the flat spacetime, $\mathbf{R}_{v_F}^{(2,1)}$, that mimics the laboratory frame.

Another issue that is possible to face with the choice (71) is that of the inequivalent quantization schemes for fields in the presence of curvature. When we use the continuum field approximation to describe the dynamics of the electrons of the π orbitals of graphene, we not only need to demand the wavelengths to be bigger than the lattice length, $\lambda > 2\pi\ell$, we also (and, perhaps, most importantly) need to have the conditions for the existence of unitarily inequivalent vacua, the most distinctive feature of QFT (on the general issue see, e.g., [19,20], and, for an application to supersymmetry breaking, see [57]). Only then can we be confident to have reobtained the necessary conditions for typical QFT phenomena to take place on a “simulating device,” as we propose graphene to be.

The matter deserves a thorough investigation [24]; nonetheless, for the moment, we can take advantage of

¹⁶Quantum gravity scenarios also might enter due to the nature of these Dirac fields, generated by a more elementary (and discrete) structure of the spacetime itself.

the results of [25]. There it is proved that, when the singularity associated with a conical defect is properly taken into account, through the self-adjoint extension of the Hamiltonian operator, inequivalent quantization schemes naturally emerge in graphene. This inequivalence is of the same topological nature as the one arising in the quantization of a particle constrained to move on a circle [26]. Thus, although the system in point has a finite number of degrees of freedom, the Stone–von Neumann theorem of quantum mechanics is violated much in the same way as for a system with an infinite number of degrees of freedom [58]. We shall not make direct use of those results here, but our logic, in this respect, is as follows.

In this paper, we are interested in reproducing the conditions for a standard QFT in a curved spacetime description of the electronic properties of graphene. As clarified before, this means that we shall focus on the effects of the intrinsic curvature, so that the action to consider can be taken to be the standard action (10). For the hexagonal lattice of graphene, intrinsic curvature means disclination defects, five-folded for positive curvature and seven-folded for negative curvature. Those are topological defects, carrying a singularity of a similar nature as the one associated with the conical defects [see, e.g., [25], and our discussion around Eq. (6)]. Hence, intrinsic curvature here is tightly linked to the unitarily inequivalent representations necessary for a proper QFT in curved spacetime. With this in mind, we take for granted here that quantum vacua associated with the curved graphene spacetime in point, e.g., the Beltrami spacetime, are unitarily inequivalent to the quantum vacuum associated with the flat graphene spacetime of interest. Furthermore, we assume that the Rindler vacuum (emerging in the way illustrated in the previous section, when negative curvature is present), and the Minkowski vacuum are too. This last assumption relies on the fact that this fictitious Rindler spacetime emerges also from the curvature of the graphene sheet, and hence the topological inequivalence mentioned above applies here too.

The assumptions described in this section are summarized in Fig. 7 for the case of the Beltrami spacetime, and for a STM measurement. The STM closely follows the profile of a Beltrami pseudosphere; hence the spatial coordinates are the same for both, the ψ electrons on the surface and the tip of the STM. The time label, t , is also the same for both, but it enters a “Beltrami time” (related to the Rindler time; see previous section) when considered from the ψ -electron point of view, and it enters a Minkowski time when considered from the laboratory point of view. This hybrid situation is taken care of by the choice of the vacuum. The “curved” electron, ψ^B (the wavy line), is supposed to tunnel into the measuring device and is indicated in the zoomed part of the figure (the circle in the middle). The final stage is indicated at the far right, Fig. 7(c). There the “ ψ description” ceases to be valid, and we are left with standard electrons. The core of the

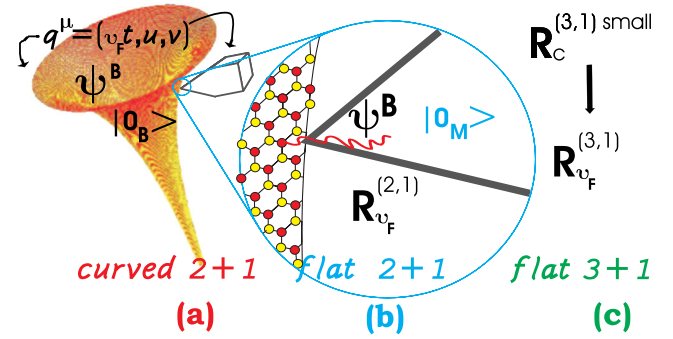


FIG. 7 (color online). A graphene quasiparticle (wavy line) enters the measuring device [the tip of a scanning tunneling microscope (STM) in the picture], from the Beltrami spacetime (this is obtained by properly setting the polarity of the bias voltage of the STM). This quasiparticle is described by a (pseudo) relativistic, massless, Dirac field, ψ^B , living in a $(2+1)$ -dimensional curved spacetime (a). Provided the tip closely follows the surface, geometrically the device has the same coordinates q^μ as the Beltrami spacetime, but the quantum vacuum of reference for it is the inertial (flat) $(2+1)$ -dimensional vacuum $|0_M\rangle$ for the Dirac field ψ with action (4) (b). This model for the measuring process takes into account that what is moving along worldlines of a curved spacetime, from the point of view of the electrons on graphene, is, at the same time, part of an inertial frame, from the point of view of the laboratory.

assumptions is in Fig. 7(b), and, as explained, it consists of modeling the measuring process as an hybrid (i) of an operation happening in the graphene curved spacetime (same q^μ for graphene and for the device), and (ii) of setting a Minkowski vacuum $|0\rangle_M$ (relative to $\mathbf{R}_{v_F}^{(2,1)}$) as the vacuum of reference during the measuring process. The latter vacuum is assumed to be nonequivalent to $|0\rangle_B$ (and to $|0\rangle_R$).

VII. THE HAWKING EFFECT ON GRAPHENE

As shown in Sec. 5, we can reproduce, on suitably curved graphene sheets, conditions for the existence of event horizons. These horizons coincide, within experimental limits, with the “end of the world” represented by the Hilbert horizon. The appearance of the cosmological type of horizon, and even the fact that a BTZ black-hole horizon might be in sight, together with the fact that the physical end of (any) surface (always) comes with a potential barrier, indicates that, when the QFT description of action (10) and of the quantum vacuum of the previous section holds, the mechanisms of pair creation and quantum tunneling through the horizon should take place here too, giving rise to a Hawking type of effects, interpreted in the spirit of Parikh and Wilczek [59]. In this approach, the other side of the horizon (the “out” region) is beyond where the surface has ended. The entanglement, necessary for the effect to take place, is between the particle that has left the

graphene membrane and the hole/antiparticle that it has left behind, and vice versa.

Although we evoked also other types of horizons, the cleanest horizon we have found is of the Rindler type (see Sec. 5 A), and hence we shall focus on that one. The entanglement now is between particles (antiparticles) of one wedge and the corresponding antiparticles (particles) of the other wedge. The above picture holds all the way. One needs to consider that, after a long enough Rindler time η (future or past null infinity, for particles and antiparticles, respectively) the particles/antiparticles reach the Hilbert/event horizon (see discussion about the geodesics of Beltrami spacetime in Sec. 5), and, through quantum tunneling, leave the surface, giving rise to the same mechanism described above. Recall that, in the mathematical limit $c \rightarrow 0$, the future/past null infinity is reached always, $\eta = r/ct$. For the physical case $c = \ell$, the lab time t it takes to reach the horizon is still short (see [9]), but the best interpretation of this fact is to say, yet from another perspective, that the effect takes place for particles and antiparticles of very small energy, $E \sim 1/\eta$, i.e., of very large wavelength, namely, large enough to feel the curvature effects $\lambda > r$.

In what follows, we shall focus on the two point Green function for the Beltrami spacetime that is related to the important measurable quantity LDOS. We shall refine the results on the Hawking effect obtained in [9] by including the role of the c parameter in the analysis and by considering the effects on the Green function of having a boundary that takes into account the reduced range of ξ with respect to the standard Rindler case. This latter instance is a manifestation, in the ideal case, of the peculiarities of the Rindler spacetime Weyl related to the Beltrami spacetime (see Sec. 5 A), while, in the practical case, it also faces the effects of the necessary truncation of the Beltrami pseudosphere in laboratory realizations.

We shall then conclude this section by briefly considering the case of a generic surface of constant negative Gaussian curvature.

A. The Hawking-Unruh effect reproduced on the Beltrami pseudosphere

We shall focus on the one particle Green function that contains all the information on the single particle properties of the system such as the LDOS, lifetime of the quasi-particles and thermodynamic properties (specific heat). For the reasons illustrated above (see the previous section), for us this function is defined as

$$S^{(B)}(q_1, q_2) \equiv \langle 0_M | \psi^{(B)}(q_1) \bar{\psi}^{(B)}(q_2) | 0_M \rangle, \quad (72)$$

where with B we indicate the reference to the Beltrami spacetime, and $q^\mu = (t, u, v)$. That is the *positive frequency Wightman function*, in the language of QFT in curved spacetimes [21–23]. To obtain this function, as announced

and prepared all along this paper, we use local Weyl symmetry of the action (10), as this case is a perfect match for its implementation [8]

$$g_{\mu\nu}^{(B)} = \phi^2(u) g_{\mu\nu}^{(R)}, \quad \psi^{(B)} = \phi^{-1}(u) \psi^{(R)}, \quad (73)$$

with (see Sec. 5 A) $\phi(u) = \ell/r e^{u/r}$ and the Rindler type of metric

$$g_{\mu\nu}^{(R)}(q) = \text{diag} \left(\frac{r^2}{\ell^2} e^{-2u/r}, -\frac{r^2}{\ell^2} e^{-2u/r}, -r^2 \right) \quad (74)$$

that was studied in detail earlier. The point we want to make here is that local Weyl symmetry allows us to translate the problem of computing (72) to the much easier task of computing

$$S^{(R)}(q_1, q_2) \equiv \langle 0_M | \psi^{(R)}(q_1) \bar{\psi}^{(R)}(q_2) | 0_M \rangle, \quad (75)$$

because

$$S^{(B)}(q_1, q_2) = \phi^{-1}(q_1) \phi^{-1}(q_2) S^{(R)}(q_1, q_2). \quad (76)$$

Thus, our goal now is to compute (75).

First let us recall once more the peculiarity of the Rindler-like spacetime (74). The time coordinate, in both wedges, ranges as usual, $\eta \equiv (r/\ell)t \in [-\infty, +\infty]$, while the relevant space coordinate, *taken for curvatures that give a good* $\xi_{Hh} \simeq \xi_{Eh}$ (see Table I), ranges as follows:

$$\xi \equiv -\frac{r}{\ell} u \in [\sim -\infty, 0] \quad \text{and} \quad \xi \equiv \frac{r}{\ell} u \in [0, \sim +\infty], \quad (77)$$

in the right wedge and in the left wedge, respectively. Of course, everywhere, $v \in [0, 2\pi]$. In both cases, $\alpha(\xi) = a e^{-a\xi}$, but, in the right wedge, $a \equiv \ell/r^2 > 0$, whereas in the left wedge, $a = -\ell/r^2 < 0$. The proper time is

$$\tau = e^{a\xi} \eta = \frac{r}{\ell} e^{-u/r} t. \quad (78)$$

The ranges of ξ in (77) indicate that we are in a case where a boundary is present at $\xi = 0$, and when computing the Green function (75) we need to take into account that the degrees of freedom of the quantum field ψ , beyond that value of ξ , are absent. It is worth recalling that $\xi = 0 = u$ corresponds here to the smallest possible value of the radius of the pseudosphere (see Fig. 3) that we set as $R(0) = \ell$.

As explained in Sec. 5 A, at $\xi = 0$, the proper acceleration is well approximated with $\alpha \simeq 0$; i.e., it corresponds to the inertial observer. Now we require that the measuring procedure on the Beltrami spacetime reproduces, on the associated Rindler spacetime just recalled, the conditions for a worldline of constant acceleration. That is simply

$$\xi = \text{const}, \quad (79)$$

which means to keep the tip of the STM at a fixed value of the meridian coordinate u , as explained also in Fig. 7 and around there. So, at any given measurement, the distance to which one has to compare how far is the boundary b is $d(\xi) = \alpha^{-1}(\xi) - r$; see (60). Thus b , measured in units of $d(\xi)$, is

$$b(0) \simeq 1 < b(\xi) < +\infty \simeq b(\xi_{Eh}). \quad (80)$$

We expect that the effects of the boundary are negligible (the boundary is too far away) when the measurements are taken near the Hilbert/event horizon ξ_{Eh} and when b is located at $\xi = 0$, which is the ideal case of a nontruncated surface. On the other hand, the boundary term also takes into account the practical issue that the Beltrami surface, when realized with the monolayer graphene, might be truncated before $\xi = 0$. It must be clear that all the computations are done for the worldline of constant acceleration, so that the conditions for the Unruh effect on the Rindler-like spacetime are fulfilled. Hence ξ is going to be constant all over.

With this in mind, the Green function $S^{(R)}$ that we have to compute needs be evaluated at *the same point in space and at two different times*, $S^{(R)}(t, \mathbf{q}, \mathbf{q}) \equiv \langle 0_M | \psi^{(R)}(t_1 = 0; \mathbf{q}) \bar{\psi}^{(R)}(t_2 = t; \mathbf{q}) | 0_M \rangle$, where the dependence on $t_2 - t_1 \equiv t$ is a result of the stationarity of the worldline in point, and we have set the initial time to zero. Eventually, what we have to consider is

$$S^{(R)}(\tau, \mathbf{q}, \mathbf{q}), \quad (81)$$

where the proper time is related to t through the relation (78), and, for the Green function to be a proper positive frequency Wightman function (see [21,22]), we need to evaluate it at $\tau \rightarrow \tau - i\epsilon$, with ϵ an infinitesimal positive parameter. This also takes into account the nonzero size of the detector.¹⁷

The power spectrum one obtains from $S^{(R)}$ is [21,22]

$$F^{(R)}(\omega, \mathbf{q}) \equiv \frac{1}{2} \text{Tr} \left[\gamma^0 \int_{-\infty}^{+\infty} d\tau e^{-i\omega\tau} S^{(R)}(\tau, \mathbf{q}, \mathbf{q}) \right], \quad (82)$$

and, for graphene, besides inessential constants, it coincides with the definition of the electronic LDOS [37,61], $\rho^{(R)}(\omega, \mathbf{q}) \equiv \frac{2}{\pi} F^{(R)}(\omega, \mathbf{q})$. This is not yet the *physical LDOS*, as the latter is only obtained once we move to the Beltrami spacetime. Nonetheless, because of Weyl symmetry, the latter step is very simple since the Weyl

¹⁷For the STM experiment we have in mind, ϵ is the size, in “natural units,” of the STM needle or tip. For a tungsten needle $\epsilon \sim 0.25 \text{ nm} \times v_F^{-1} \sim 10^{-10} \text{ s}$, while for a typical tip $\epsilon \sim 10 \text{ \AA} \times v_F^{-1} \sim 10^{-15} \text{ s}$ (see, e.g., [60]). Those values of ϵ are indeed infinitesimal.

factor in (76) is time independent, and it goes through the Fourier transform, i.e., $F^{(B)}(\omega, \mathbf{q}) = \phi^{-2}(\mathbf{q}) F^{(R)}(\omega, \mathbf{q})$, with obvious notation; hence the physical LDOS is

$$\rho^{(B)}(\omega, \mathbf{q}) = \phi^{-2}(\mathbf{q}) \rho^{(R)}(\omega, \mathbf{q}). \quad (83)$$

Thus, the only necessary computation is that of $F^{(R)}$ in (82).

A direct computation of $F^{(R)}$ might be an interesting calculation to perform in the future, because it might help in clarifying the physical structure of the vacuum condensate. Nonetheless, having carefully identified how to translate all the peculiarities of this system into the proper QFT counterparts, we have recast such a computation to that of a very well-known case. We shall, then, resort to the exact results (zero mass) obtained, e.g., in [22]. It should be clear that, if one uses the identical overall conditions we have (i.e., the Minkowski vacuum and the spacetime of Sec. VA), the direct computation is bound to give the same results. Hence, since our main interest here is not to probe into the vacuum structure, but rather to produce a testable prediction of the measurable LDOS, such direct calculation is redundant, and we shall not perform it here.

Let us recall the main steps. First one uses the fact that, in general, and for any spacetime dimension n , the Dirac (S_n) and scalar (G_n) Green functions are related as $S_n = i\partial G_n$ (here $m = 0$). With our choice of the worldline (i.e., for us, of the measuring procedure) we then have the exact expression

$$S_n^{(R)}(\tau) = \gamma^0 \partial_z G_n^{(R)}(\tau) = \gamma^0 \lambda_n G_{n+1}^{(R)}(\tau), \quad (84)$$

where $z = \epsilon + 2i\alpha^{-1} \sinh(\alpha\tau/2)$ and $\lambda_n = 2\sqrt{\pi} \times \Gamma(n/2)/\Gamma((n-1)/2)$; see [22]. Thus, we see here that to compute our three-dimensional Dirac Green functions we need a four-dimensional scalar field. By taking in (84) $n = 3$, the Fourier transform, and the trace, as in (82), one easily obtains

$$F^{(R)}(\omega) \equiv F_3^{(R)}(\omega) = \lambda_3 B_4^{(R)}(\omega), \quad (85)$$

where $B_4^{(R)}(\omega)$ is the power spectrum of the four-dimensional scalar field. Thus what is left to compute is

$$B_4^{(R)}(\omega) \equiv B_{\text{thermal}}^{(R)}(\omega) + B_{\text{boundary}}^{(R)}(\omega), \quad (86)$$

which is made of two parts, one showing thermal features and one due to the presence of the boundary in b , and this splits into two all relevant quantities, $F^{(R)}$, $F^{(B)}$, $\rho^{(R)}$, and the most important $\rho^{(B)}$.

The expression for $B_{\text{thermal}}^{(R)}(\omega)$ has been obtained in many places. Here we use the notation of [22] that gives (see also [9]) $B_{\text{thermal}}^{(R)}(\omega) = (\omega/2\pi)/(e^{2\pi\omega/\alpha} - 1)$. Using this in (85), one immediately obtains

$$F_{\text{thermal}}^{(R)}(\omega, \mathbf{q}) = \frac{\omega/2}{e^{2\pi\omega/\alpha} - 1}, \quad (87)$$

where we used $\lambda_3 = \pi$, an Unruh type of temperature appears [62], and α is positive [22] [see also discussion after (92) below],

$$\mathcal{T} \equiv \frac{\hbar v_F}{k_B} \frac{\alpha}{2\pi} = \frac{\hbar v_F}{k_B} \frac{\ell}{2\pi r^2} e^{u/r}, \quad (88)$$

with $u \in [0, r \ln(r/\ell)]$, and where the proper dimensional units were reintroduced and a Tolman factor [52] $e^{u/r} = e^{-a\xi}$ appears, as required by local measurements. The expression for the thermal part of the physical LDOS is then immediate [recall that $\phi(u) = \ell/r \exp(u/r)$],

$$\rho_{\text{thermal}}^{(B)}(E, u, r) = \frac{4}{\pi} \frac{1}{(\hbar v_F)^2} \frac{r^2}{\ell^2} e^{-2u/r} \frac{E}{\exp[E/(k_B \mathcal{T}(u, r))] - 1}, \quad (89)$$

where we included the $g = 4$ degeneracy and the proper dimensions, e.g., $\omega \equiv \omega/v_F$, $E \equiv \hbar\omega$. This is the LDOS when boundary effects are absent.

The form of (89) is the same as the corresponding one obtained in [9], as can be seen from Fig. 8, where we plot $\rho_{\text{thermal}}^{(B)}$ vs E , within the range of validity of our model, $|E| < E_r$, for three different values of u . There are, though, some differences of interpretation, with respect to [9], due to $c = \ell$. The largest temperature

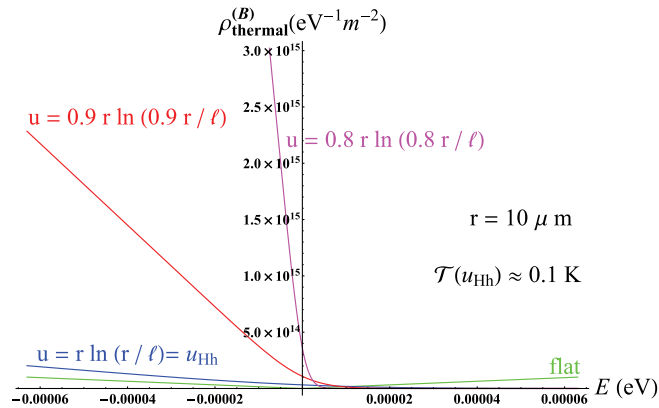


FIG. 8 (color online). Plots of the thermal LDOS against E , within the range of validity of our model, $|E| < E_r \sim 6.3 \mu\text{eV}$. The curves are for the indicated values of the u coordinate on the Beltrami surface and for a fixed radius of curvature $r = 10 \mu\text{m}$. We also plot the flat LDOS for comparison. This plot is in all respects an important one, the same as the corresponding plot of [9]. The only key difference lies in the fact that, due to the role of $c = \ell$, the Hilbert horizon plays a more prominent role. The indicated temperature is the maximal temperature, reached at the horizon, where $u = r \ln(r/\ell) = u_{\text{Hh}}$. The temperatures corresponding to the other curves become increasingly smaller, according to the expression (88).

\mathcal{T} is still reached at the Hilbert horizon, and the value is the same here and there

$$\mathcal{T}(r \ln(r/\ell)) = \frac{\hbar v_F}{k_B} \frac{1}{2\pi r}, \quad (90)$$

but now the Hilbert and event horizons coincide. Notice also that in (89) the factor $r^2/\ell^2 \sim +\infty$ is fully balanced by the exponential factor next to it, $e^{-2u/r}$, only on the horizon $u = r \ln(r/\ell)$,

$$(r^2/\ell^2) e^{-2u/r} \Big|_{u=r \ln(r/\ell)} = 1, \quad (91)$$

as could have been guessed by the fact that $\phi|_{\text{horizon}} = 1$; see footnote 14. These facts clarify that what we have learned here is that the interesting phenomena happen near the horizon. More indications of this come from the considerations of the effects of the boundary, which we shall face next.

A complete calculation of the effects of the boundary would need the full knowledge of how the surface truly ends on the thin side, and of how that can be described in terms of our Rindler spacetime. There is an entire literature on the effects of various shapes and locations of boundaries and mirrors on the Unruh effect; see, e.g., [63] and references therein. Here we shall follow [64], and we shall consider the case of the static boundary in b . The formula we shall obtain must not be trusted in all details but will serve well the scope of showing how the nonthermal features of the LDOS do not necessarily mean that our approach, based on QFT in curved spacetime, is not working. In fact, those nonthermal features can be understood within this model.

The positive frequency Wightman function, for a four-dimensional scalar field, evaluated along a worldline of constant acceleration (that is the one obtained by measuring at a fixed meridian coordinate on the surface), in the presence of one static boundary, located at a (dimensionless) distance b , in units of the distance of the point of measurement from the horizon (see earlier discussion), is given by [64]

$$G_{\text{boundary}}^{(R)}(\tau, b) = -\frac{1}{4\pi^2} \frac{\alpha^2}{4} \frac{1}{[\cosh(\alpha\tau - i\varepsilon) - b]^2}. \quad (92)$$

This result, as it stands, is for one boundary in one sector (wedge) only. To adapt the results of [64] to our case, we also need to consider another boundary in a symmetric position, in the other sector (wedge). As explained at the beginning of this section, our picture here is that the other wedge is obtained by the existence of antiparticles, for which the time flows in opposite directions, hence the meaning of positive and negative frequency swap. Thus what we have to do is consider both the positive frequency and the negative frequency Wightman functions, and keep

both α and b positive. By doing this, and by using the general procedure to obtain the LDOS discussed earlier (see [28] for details), the result one obtains is

$$\rho_{\text{boundary}}^{(B)}(E, u, r) = \frac{2}{\pi} \frac{1}{(\hbar v_F)^2} \frac{r^2}{\ell^2} e^{-2u/r} \frac{|E|}{b^2 - 1} \cos\left(\tilde{b} \frac{E}{\hbar v_F \alpha(u, r)}\right), \quad (93)$$

where $\tilde{b} = \text{arcosh} b$. The behavior of the boundary term is as expected,

$$\rho_{\text{boundary}}^{(B)} \rightarrow 0 \quad \text{for } b \rightarrow +\infty \quad \text{and} \quad \rho_{\text{boundary}}^{(B)} \rightarrow \pm\infty \quad \text{for } b \rightarrow 1. \quad (94)$$

Indeed, the first limit describes the case of infinite distance, in units of α^{-1} , between the point u where one measures and the value of u where the surface ends, which is a measurement taken near the Hilbert horizon, $R = r$, and the thin end of the surface ending at $R = \ell$. The second limit refers to a measurement taken on/near the boundary itself. There our approximations for the boundary do not hold fully; nonetheless we can trust that the boundary there will, of course, dominate. Let us stress again that the boundary term (93) takes into account the fact that the infinities here are only approximated. This has two meanings. First, even in the ideal case of a Beltrami that ends at $R = \ell$ (and supposing that our QFT approximations work till there),

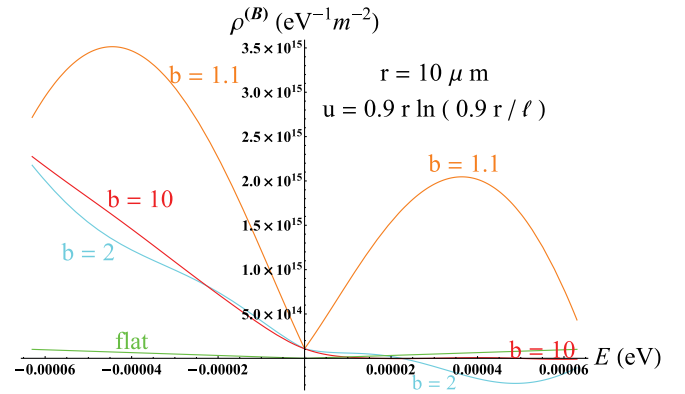


FIG. 9 (color online). Plots of the total LDOS against E , within the range of validity of our model, $|E| < E_r \sim 6.3 \mu\text{eV}$. The curves are for the indicated three values of b , for a fixed value of $u = 0.9r \ln(0.9r/\ell)$, and for the same fixed radius of curvature of Fig. 8 $r = 10 \mu\text{m}$. We also plot the flat LDOS. The plot for $b = 10$ here (in red) should be compared with the thermal plot for the corresponding value of u in Fig. 8 (in red there, too).

the range of u is not really infinite. Second, the real graphene surface will end before that ideal value of R anyway. What is important, though, is to see how strong are the nonthermal corrections over the thermal spectrum. To see it, let us write the total LDOS for a graphene membrane shaped as a Beltrami pseudosphere that, in our model, then reads

$$\rho^{(B)}(E, u, r) = \frac{4}{\pi(\hbar v_F)^2} \frac{r^2}{\ell^2} e^{-2u/r} \left[\frac{E}{\exp[(2\pi E)/(\hbar v_F \alpha(u, r))] - 1} + \frac{1}{2} \frac{|E|}{b^2 - 1} \cos\left(\frac{\tilde{b} E}{\hbar v_F \alpha(u, r)}\right) \right]. \quad (95)$$

In Fig. 9 we plot $\rho^{(B)}$ vs E , for different values of b , for a fixed value of $u = 0.9r \ln(0.9r/\ell)$, and for the same fixed radius of curvature of Fig. 8. For values of b close to 1, the boundary term dominates, and the thermal nature is gone. The negative values of $\rho^{(B)}(E)$, in those cases, need not be taken too seriously, as our approximations do not allow us to trust the formula in all details too near the extremal values of $b = 1$. What is important here is that, for relatively small values of b , the thermal character is practically untouched. Indeed, compare the plot for $b = 10$ in Fig. 9 (in red) with the thermal plot for the corresponding value of u in Fig. 8 (in red there, too).

To have a flavor of what these values correspond to in practice, let us indicate with \bar{u} the point of measurement, and let be $\bar{u} \equiv f u_{Hh}$, with $f < 1$. Then, one defines u_b as the value of u such that the Rindler distance d [see (60)] of the boundary from the horizon is b times the Rindler distance d from the horizon of \bar{u} . With these, $u_b = -r \ln \left[\frac{\ell}{r} (b((\ell/r)^{f-1} - 1) + 1) \right]$, which for $f = 0.9$ and $r = 10 \mu\text{m}$, as in Fig. 9 gives for $b = 10$ a

$u_b \simeq 81 \mu\text{m}$. This means that of the whole surface, whose u length, $r \ln(r/\ell)$, is about $115 \mu\text{m}$, only about 30% is necessary. This is a small portion of the Beltrami surface; nonetheless, the spectrum is very well approximated by a thermal spectrum. The closer to the horizon we measure, the less surface is necessary, and the more reliable are our approximations. For instance, when $f = 0.99$, for $b = 10$, even just 4% of the surface is enough. On the other hand, when $f = 0.1$, to reach $b = 10$ we need to continue the surface beyond $u = 0$, corresponding to $R = \ell$, because u_b becomes negative. This indicates that our formula works well for measurements taken near the horizon and that thermal effects should be easy to obtain there.

As a side note, let us add that, in the formula (95), we emphasized the role of $\alpha = (\ell/r^2) \exp(u/r)$, which, boundary effects permitting, is related to the temperature, as in (88), but we could have, as well, focused on entirely geometrical quantities. In this latter case we would have noticed that the constant v_F always appears next to a factor $\exp(u/r)$; hence we have an effective Fermi velocity that is space dependent

$$v_F(u) \equiv v_F e^{u/r} \quad \text{with} \quad u \in [0, r \ln(r/\ell)], \quad (96)$$

in agreement with what was announced in Sec. 2 (see footnote 4) and with the literature [37]. Of course, the effects of the lattice, like anisotropy, v_F^{ij} (see [47]), do not appear here, due to our focusing on the very large wavelengths/very small energies. Nonetheless, we do not know how seriously we can take (96) as, for the values of r in which we are interested, $v_F(u)$ soon becomes greater than the speed of light.

B. The Hawking effect for a generic surface of constant negative \mathcal{K}

Can we have a Hawking effect also on a generic surface Σ of constant negative \mathcal{K} , besides the Beltrami? And, can the results of the previous section be used? The answers are, in general, affirmative: *If on Σ the conditions for an event horizon are realized, then a Hawking effect, of the kind described at the beginning of this section, takes place and manifests itself, e.g., through a LDOS whose structure is the same as the LDOS (95) of the Beltrami surface.* In practice, though, it might be quite complicated to have control of the procedure, especially of the all important occurrence of the event horizon.

Let us now show why this is so, what the issues are, as well as a possible strategy to see whether the effect is there. The line element of the spacetime is (32)

$$ds^2 = \frac{r^2}{\tilde{y}^2} \left[\frac{\tilde{y}^2}{r^2} dt^2 - d\tilde{y}^2 - d\tilde{x}^2 \right],$$

where the abstract Lobachevsky coordinates need be specified for Σ : $\tilde{x}_\Sigma(u_\Sigma, v_\Sigma)$ and $\tilde{y}_\Sigma(u_\Sigma, v_\Sigma)$, including the ranges of u_Σ and v_Σ . Now, as recalled earlier (see Sec. 4.2 and [13]) *any* Σ is locally reducible to one of the three pseudospheres; i.e., its line element can be reduced to the line element of one of the three pseudospheres. In this paper we have shown that, in the limit for $c \rightarrow 0$, the three pseudospheres all become the Beltrami¹⁸ (see Sec. 4.2) with some global differences that can become important for the existence of a well defined Hilbert horizon on Σ . At any rate, *locally*, by considering Beltrami in the $c \rightarrow 0$ limit, we are dealing also with Σ *in the same limit*. Indeed, after the reduction of the line element of Σ , c is in $dl_\Sigma^2(c)$ too; hence we can obtain the shape of Σ in that limit by knowing how the ranges of $u_\Sigma(c)$ and $v_\Sigma(c)$ are affected.

¹⁸Notice that, since we are always referring to the Beltrami spacetime, the type of horizon we are considering is of the Rindler type. One might as well use, say, the elliptic pseudosphere as a reference; hence the horizon would be of the cosmological kind. Although interesting, this case is less appealing for our purposes as the spacetimes would be Weyl related to nonflat spacetimes, de Sitter; hence the formula (95) would not be of direct use.

When, on Σ , a Hilbert horizon is well defined by the coordinates $(u_\Sigma^{Hh}, v_\Sigma^{Hh})$ and when, for $c \rightarrow 0$, $\tilde{y}_\Sigma(u_\Sigma^{Hh}, v_\Sigma^{Hh}) \simeq 0$ (see discussion in Sec. 5), it is within physically reasonable approximations, then the event horizon is present on Σ , and it coincides, within the same approximations, with its Hilbert horizon $u_\Sigma^{Eh} \simeq u_\Sigma^{Hh}$ and $v_\Sigma^{Eh} \simeq v_\Sigma^{Hh}$. What we cannot know *a priori* is whether indeed there is a good Hilbert horizon on Σ . The embedding in \mathbf{R}^3 that gives Σ can be so intricate that the Hilbert horizon might be a meaningless concept there, even though it might be mapped onto meaningful ones, $R = r$, or $R = r \cos \vartheta$, or $R = \sqrt{r^2 + c^2}$, and then, eventually, to the $R = r$ of Beltrami.

Summarizing, if we know that a Hilbert horizon exists on Σ , and we know the mapping from Σ to “its pseudosphere”

$$u_\Sigma(u_p, v_p) \quad \text{and} \quad v_\Sigma(u_p, v_p), \quad (97)$$

where p stands for any one of the three pseudospheres, we know how c enters the line element and the ranges of u_Σ and v_Σ , so that we can perform the limit $c \rightarrow 0$ and we shall know the resulting shape of Σ and the location of its Hilbert horizon, which will coincide with an event horizon. Furthermore, in that limit, the pseudosphere of reference has become the Beltrami; hence the formula (95) can be used

$$\rho^{(\Sigma)}(E, u_\Sigma, v_\Sigma) \simeq \rho^{(B)}(E, u_B(u_\Sigma, v_\Sigma)), \quad (98)$$

where $u_B(u_\Sigma, v_\Sigma)$ is obtained by inverting (97), after the limit $c \rightarrow 0$ has been performed. But there is a *crucial warning* for the correct use of formula (98): *The formula is valid only locally.* That is why we use “ \simeq .” Because of the local nature of the geometric reduction of Σ to the pseudosphere, the mapping (97) might be multivalued (hence not a true map). That means that, if we insist in using the formula for a closed path on Σ , the formula might give different values for the same point at each full turn, an instance that has no physical meaning. Hence, in general, we can only use (98) in a small neighbor for the given point of measurement (u_Σ, v_Σ) . Recall that we have encountered already problems of multivaluedness (see Sec. 4.2), due to the choice of coordinates we have constrained ourselves to use. That problem, and this too, in principle might be solved by a clever choice of new coordinates [see, e.g., (39) and (40)], but then one needs to explain the physics of their realization in the laboratory.

Another issue with the use of (98) is more practical. Because of the nature of the mapping, it might happen that measuring at a given point, (u_Σ^1, v_Σ^1) , one sees thermal effects, while measuring at a close point, (u_Σ^2, v_Σ^2) , the thermal effects are gone. Indeed, close points on Σ might correspond to far points on Beltrami, and hence the effects of the boundary term might unexpectedly play the role of masking the Hawking effect that is, in fact, present.

VIII. CONCLUSIONS

We have put on the table the fundamental issues arising when realizing with curved graphene a QFT in curved spacetime, have found solutions to some of these issues, have pointed to the open problems, and have consequently produced predictions of measurable Hawking-Unruh effects. The whole construction is behind the formula (95) for the LDOS that is valid for a (truncated, hence realistic) Beltrami pseudosphere. Of course, a real graphene system may be subject to the effect of the substrate, or of surface polaritons and plasmons, that may affect the signal for this Hawking-Unruh effect. Part of these unwanted effects can be removed either by using inert substrates or by performing idealized computer simulations where the wanted shape is realized.

The use of Weyl symmetry, of Lobchevsky geometry, of known correspondences of the differential geometry of surfaces, and of our own results makes us then conclude that the Beltrami case contains crucial information on the general case. Hence, although the matter is only sketched here, we can indicate a prediction for the general case, which is the expression (98) for the LDOS.

ACKNOWLEDGMENTS

We thank F. Azariadis, I. Carusotto, G. Gibbons, G. Giribet, F. Guinea, R. Jackiw, A. MacDonald, A. Marzuoli, V. Moretti, N. Nicolaevici, P. Pais, G. Palumbo, M. Politi, D. Rastawicki, A. Recati, F. Scardigli, S. Sen, G. Silva, G. Vitiello, M. Vozmediano, J. Zanelli, and A. Zelnikov for interacting with us on different aspects and at different stages of this research. A.I. acknowledges the kind hospitality of the Departments of Physics of University of Buenos Aires, of University of Salerno, and of University of Trento, where parts of this work were carried on, and he also thanks R. Leitner for extensive financial support. A.I. wishes to thank the Czech Science Foundation (GACR) for support through Contract No. 14-07983S. G.L. wishes to thank the Agenzia Spaziale Italiana (ASI) for partial support through the ASI Contract No. I/034/12/0.

APPENDIX A: THE COSMOLOGICAL-LIKE HORIZON OF BELTRAMI SPACETIME FROM THE ELLIPTIC PSEUDOSPHERE (DE SITTER) SPACETIME

In this Appendix and in the next one, we should evoke two spacetimes, de Sitter, which is important for cosmology, and BTZ, which is a black-hole spacetime, respectively. Our main scope is to illustrate how the same Hilbert horizon of the Beltrami spacetime, besides being Weyl related to the Rindler-like event horizon, is also Weyl related to the event horizon of those two spacetimes. Thus, although we shall establish links between important physical quantities on both sides (the de Sitter/BTZ side and the

graphene side), we shall present here only a kinematical starting point for a much deserved study that probes full power into those analogies.

De Sitter (dS) spacetime, in $(2 + 1)$ dimensions, can be described by the following line element:

$$ds_{\text{dS}_3}^2 = (1 - \mathcal{R}^2/r^2)dt^2 - (1 - \mathcal{R}^2/r^2)^{-1}d\mathcal{R}^2 - \mathcal{R}^2dv^2, \quad (\text{A1})$$

where t and v are the time and angular variables, respectively, and \mathcal{R} is the radial coordinate. The positive quantity r is related to the cosmological constant through $\Lambda = 1/r^2 > 0$; hence, through the relation Ricci = 6Λ , valid in $(2 + 1)$ dimensions, the Ricci scalar curvature is $+6/r^2$. Clearly, this spacetime has an event horizon at $\mathcal{R}_{\text{eh}} = r$. After the discovery of the positive (but tiny) value of the cosmological constant, this spacetime became of great importance for nowadays cosmology. Its horizon is often referred to as ‘‘cosmological horizon,’’ i.e., the horizon that limits what we can observe of the expanding universe, due to the finiteness of the speed of light (see, e.g., [55]). We shall not probe into this here.

On the other hand, anti-de Sitter (AdS) spacetime, in $(2 + 1)$ dimensions, can be described by substituting $r \rightarrow ir$ in (A1)

$$ds_{\text{AdS}_3}^2 = (1 + \mathcal{R}^2/r^2)dt^2 - (1 + \mathcal{R}^2/r^2)^{-1}d\mathcal{R}^2 - \mathcal{R}^2dv^2, \quad (\text{A2})$$

so that it has negative cosmological constant $\Lambda = -1/r^2 < 0$, and Ricci scalar curvature $-6/r^2 < 0$. As is evident, this spacetime does not have an intrinsic horizon. We shall now show that our spacetimes of constant *negative* curvature are related to the dS rather than the AdS spacetime.¹⁹

A standard way to introduce both spacetimes is through the embedding into higher $[(3 + 1)$ in this case] dimensional flat spacetimes. The two spacetimes are the solutions to these equations

$$\eta_{AB}x^Ax^B = +r^2 \quad \text{and} \quad \tilde{\eta}_{AB}x^Ax^B = -r^2, \quad (\text{A3})$$

the first for dS, and the second for AdS. Here $A, B = 0, 1, 2, 3$, $\eta_{AB} = \text{diag}(+1, -1, -1, -1)$, and $\tilde{\eta}_{AB} = \text{diag}(+1, -1, -1, +1)$, so that dS \leftrightarrow AdS when $r \leftrightarrow ir$ and $z \leftrightarrow iz$, where $x^3 \equiv z$. Usually, no physical meaning is ascribed to the higher dimensional embedding manifold but

¹⁹This result only apparently seems to contradict the discussion in [56], in relation to the possibility to have a Hawking phenomenon through an embedding procedure into flat higher dimensional spacetimes. There it is shown that the spacetimes of constant negative curvature, AdS, cannot have an intrinsic Hawking phenomenon. It is necessary to include an acceleration, $a > 1/r$, in the higher dimensional Rindler spacetime. Here, instead, the spacetimes of negative curvature are related to dS.

only to the resultant spacetime; see, e.g., [56]. Thus, a signature like that of $\tilde{\eta}_{AB}$ is not a problem. For us this cannot be the case, as we do give physical meaning to the embedding spacetime; hence we cannot have the former signature, but only the one of η_{AB} . With this in mind, what we shall now do is to consider the well-known Weyl equivalence of an AdS spacetime to an Einstein static universe spacetime.

By defining

$$\frac{1}{\mathcal{R}^2} \equiv \frac{1}{R^2} - \frac{1}{r^2} = \frac{1}{r^2 \cos^2(u/r)} - \frac{1}{r^2}, \quad (\text{A4})$$

and shifting the u variable, $u \rightarrow u + r\pi/2$, the line element in (A2) can be written as

$$ds_{\text{AdS}_3}^2 = \frac{1}{\cos^2(u/r)} [dt^2 - du^2 - r^2 \sin^2(u/r) dv^2], \quad (\text{A5})$$

where the line element in square brackets is what we have found for the spherically shaped graphene membrane, with

$R(u) = r \sin(u/r)$. The first consideration here is that, as announced earlier, when graphene is shaped in a spherical fashion, since its line element is related to the AdS spacetime, we do not expect any horizon. The second consideration is more important and is what we are looking for here.

Consider the line element obtained by substituting $r \rightarrow ir$ in (A5) and including the factor $\sin \vartheta$ to take into account the geometry of the pseudosphere

$$ds^2 = \frac{1}{\cosh^2(u/r)} [dt^2 - du^2 - (r^2 \sin^2 \vartheta) \sinh^2(u/r) dv^2]. \quad (\text{A6})$$

This is Weyl related, through the time-independent conformal factor $1/\cosh^2(u/r)$, to the graphene spacetime for the elliptic pseudosphere, in square brackets, which we have already encountered. The radius is $R(u) = c \sinh(u/r)$, with the parametrization $c = r \sin \vartheta \leq r$. Substituting $R(u)$ for u in (A6), the line element becomes

$$ds^2 = \left(1 + \frac{R^2}{r^2 \sin^2 \vartheta}\right)^{-1} \left[dt^2 - \frac{1}{\sin^2 \vartheta} \left(1 + \frac{R^2}{r^2 \sin^2 \vartheta}\right)^{-1} dR^2 - R^2 dv^2 \right] \quad (\text{A7})$$

$$\equiv \left(1 - \frac{\mathcal{R}^2}{r^2 \sin^2 \vartheta}\right) dt^2 - \frac{1}{\sin^2 \vartheta} \left(1 - \frac{\mathcal{R}^2}{r^2 \sin^2 \vartheta}\right)^{-1} d\mathcal{R}^2 - \mathcal{R}^2 dv^2 = ds_{\text{dS}_3}^2, \quad (\text{A8})$$

where

$$\frac{1}{\mathcal{R}^2} \equiv \frac{1}{R^2} + \frac{1}{r^2} = \frac{1}{(r \sin \vartheta)^2 \sinh^2(u/r)} + \frac{1}{(r \sin \vartheta)^2}. \quad (\text{A9})$$

That means that the graphene spacetime for an elliptic pseudosphere is Weyl related to a dS_3 spacetime

$$ds_{\text{Ell}}^2 = \left(1 + \frac{R^2}{r^2 \sin^2 \vartheta}\right) ds_{\text{dS}_3}^2 = \left(1 - \frac{\mathcal{R}^2}{r^2 \sin^2 \vartheta}\right)^{-1} ds_{\text{dS}_3}^2, \quad (\text{A10})$$

and an event horizon appears at

$$\mathcal{R}_{Eh} = r \sin \vartheta. \quad (\text{A11})$$

Let us clarify here that this dS spacetime is not the one produced by shaping a graphene membrane as an elliptic pseudosphere. It is only Weyl related to it through (A10). Hence, the fact that, e.g., the Ricci scalar curvature of this dS spacetime is $+6/r^2$ should not create confusion. The latter is the Ricci curvature of the Weyl-related dS spacetime, while $-2/r^2$ is the Ricci curvature of the elliptic pseudosphere spacetime, as it must be.

What we need to do is to compare this horizon with the Hilbert horizon and to use our *Ansatz* $c = \ell$, which gives

$$\vartheta = \arcsin(\ell/r). \quad (\text{A12})$$

The Hilbert horizon, in terms of the measurable radial variable R is at $R_{Hh} = r \cos \vartheta$; see previous discussions and Fig. 5 So that, from (A9), we see that in terms of the radial dS_3 coordinate, is

$$\mathcal{R}_{Hh} = \frac{1}{2} r \sin(2\vartheta). \quad (\text{A13})$$

Clearly, for small ϑ , that means small ℓ/r [see (A12)], the two horizons coincide, and they have the value

$$\mathcal{R}_{Eh} \simeq \mathcal{R}_{Hh} \simeq r \frac{\ell}{r} = \ell. \quad (\text{A14})$$

This holds for any value of r , provided this is a big enough $r > \ell$. In the same limit, the elliptic spacetime tends to the Beltrami spacetime, and, in terms of the measurable radial coordinate R , the Hilbert horizon of the former, tends to the Hilbert horizon of the latter,

TABLE II. Quantification of how good it is to approximate the Hilbert horizon of the elliptic pseudosphere spacetime with a cosmological event horizon. The closer $\zeta_{\text{Ell}} \equiv (\mathcal{R}_{\text{Eh}} - \mathcal{R}_{\text{Hh}})/r$ is to zero, the better is the approximation. We indicate three values of ℓ/r comparable to those used in Table I, the corresponding values of ζ_{Ell} , and how close the Hilbert horizon of this spacetime ($R = r \cos \vartheta$) is to the Hilbert horizon of the Beltrami spacetime ($R = r$). The latter column, then, is also a measure of how well the elliptic pseudosphere spacetime can be identified with the Beltrami spacetime. The values are all approximate.

$\vartheta \sim \ell/r$	ζ_{Ell}	$(R_{\text{Hh}} - r)/r$
0.1	5×10^{-4}	5×10^{-3}
10^{-4}	5×10^{-13}	5×10^{-9}
10^{-7}	5×10^{-22}	5×10^{-15}

$$R_{\text{Hh}}^{\text{Elliptic}} = r \cos \vartheta \rightarrow r = R_{\text{Hh}}^{\text{Beltrami}}. \quad (\text{A15})$$

In other words, the very same Hilbert horizon we have seen earlier to be related to the Rindler event horizon is also related to a cosmological dS event horizon. In Table II we show how good these approximations are for a graphene membrane.

APPENDIX B: THE BLACK HOLE-LIKE HORIZON OF BELTRAMI SPACETIME FROM THE HYPERBOLIC PSEUDOSPHERE (BTZ) SPACETIME

It was shown in [29] that the line element of the nonrotating BTZ black hole is Weyl related to the line element of the hyperbolic pseudosphere spacetime. There it was concluded that the Hilbert horizon and the event horizon could not match. For a nonextremal hyperbolic pseudosphere, strictly speaking, this is true. Nonetheless, when the geometrical/physical role of the c parameter is duly taken into account (the *Ansatz* $c = \ell$), the two horizons coincide, in the $\ell/r \rightarrow 0$ limit, although the mass of the hole goes to zero even faster. In that limit the hyperbolic pseudosphere tends to two Beltrami pseudospheres “glued” at the tails (see previous discussion and Fig. 10). Thus the correct statement here is that the Hilbert horizon of the Beltrami spacetime (that, in terms of the measurable radial coordinate, is always given by $R = r$) is also a limiting case of zero mass of a BTZ event horizon (i.e., $\mathcal{R} \sim 0$, in terms of the BTZ radial coordinate). Let us show this here.

The line element of the BTZ black hole, with zero angular momentum is [16]

$$\begin{aligned} ds_{\text{BTZ}}^2 &= \left(\frac{\mathcal{R}^2}{c^2} - M \right) dt^2 - \frac{d\mathcal{R}^2}{\frac{\mathcal{R}^2}{c^2} - M} - \mathcal{R}^2 d\chi^2 \\ &\equiv \left(\frac{\mathcal{R}^2}{c^2} - M \right) ds^2, \end{aligned} \quad (\text{B1})$$

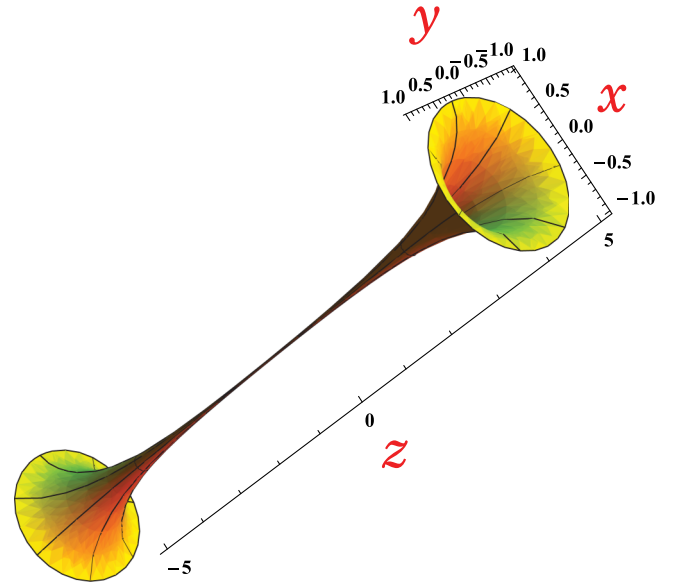


FIG. 10 (color online). The hyperbolic pseudosphere for a small value of c/r that clearly shows how the surface, for $c/r \rightarrow 0$, tends to two Beltrami pseudospheres joined at the minimum value of R . In the plot, $r = 1$, $c = 1/100$; hence, $u \in [-\text{arccosh}(\sqrt{10001}), +\text{arccosh}(\sqrt{10001})]$ and $v \in [0, 2\pi]$. The Hilbert horizons are two and are located at the two maximal circles $R_{\text{max}} \simeq 1.00005$.

where c and M are two non-negative real constants, the cosmological constant is negative, $\Lambda = -1/c^2 < 0$, and

$$ds^2 \equiv dt^2 - c^4 \frac{d\mathcal{R}^2}{(\mathcal{R}^2 - \mathcal{R}_{\text{Eh}}^2)^2} - c^2 \frac{\mathcal{R}^2}{(\mathcal{R}^2 - \mathcal{R}_{\text{Eh}}^2)} d\chi^2. \quad (\text{B2})$$

Here

$$\mathcal{R}_{\text{Eh}} \equiv c\sqrt{M} \quad (\text{B3})$$

is the event horizon of the black hole.

Let us define $\chi \equiv v$ as the angular variable,²⁰ and

$$du \equiv -\frac{c^2}{\mathcal{R}^2 - \mathcal{R}_{\text{Eh}}^2} d\mathcal{R}, \quad R(\mathcal{R}) \equiv \frac{c\mathcal{R}}{\mathcal{R}^2 - \mathcal{R}_{\text{Eh}}^2}, \quad (\text{B4})$$

from which one easily obtains

$$\mathcal{R}(u) = \mathcal{R}_{\text{Eh}} \coth(\mathcal{R}_{\text{Eh}} u / c^2) \quad (\text{B5})$$

that gives

$$R(\mathcal{R}(u)) \equiv R(u) = c \cosh(\mathcal{R}_{\text{Eh}} u / c^2); \quad (\text{B6})$$

i.e., the line element in (B2) is that of the hyperbolic pseudosphere spacetime

²⁰This identification is particularly important to turn a standard AdS_3 spacetime into the BTZ black hole; see [16], [17], [18]. Here we do not touch upon this and other important issues.

$$ds_{\text{BTZ}}^2 = \left(\frac{\mathcal{R}^2}{c^2} - M \right) ds_{\text{Hyp}}^2, \quad (\text{B7})$$

with $r \equiv c^2/\mathcal{R}_{\text{Eh}} = c/\sqrt{M}$ [see (B3)] or $M = c^2/r^2$. We now use our *Ansatz* for graphene, $c = \ell$, and write the relevant BTZ quantities after this identification

$$\Lambda \equiv -\frac{1}{\ell^2}, \quad M \equiv \frac{\ell^2}{r^2}, \quad \mathcal{R}_{\text{Eh}} \equiv \frac{\ell^2}{r}. \quad (\text{B8})$$

We now need to compare this event horizon to the Hilbert horizon of the hyperbolic pseudosphere spacetime that, in terms of the radial coordinate of the pseudosphere, is at

$$R_{\text{Hh}} = \sqrt{r^2 + \ell^2} = r\sqrt{1 + \ell^2/r^2}, \quad (\text{B9})$$

or, in terms of the meridian coordinate, $u_{\text{Hh}} = \text{rarcosh}(\sqrt{1 + r^2/\ell^2})$. Substituting this value into (B5) and using (B8),

$$\mathcal{R}_{\text{Hh}} \equiv \mathcal{R}(u_{\text{Hh}}) = \mathcal{R}_{\text{Eh}} \coth \left(\text{arcosh} \left(\sqrt{1 + r^2/\ell^2} \right) \right). \quad (\text{B10})$$

For $r = 10^n \ell$ this formula approximates to

$$\begin{aligned} \mathcal{R}_{\text{Hh}} &= \mathcal{R}_{\text{Eh}} \times \frac{10^n}{(10^{2n} - 1)^{1/2}} \\ &\simeq \mathcal{R}_{\text{Eh}} \times (1 + 5 \times 10^{-(2n+1)}). \end{aligned} \quad (\text{B11})$$

From Table III, it is clear that, again, in the small ℓ/r limit these two horizons coincide, but that is also the limit where $M \rightarrow 0$, and accordingly $\mathcal{R}_{\text{Eh}} \rightarrow 0$; i.e., the black-hole has disappeared, and we are left with what in [16] is called “the vacuum state.” This means that, in order to have a proper BTZ black hole, something different needs to be done, but we shall not probe into that here, as our scope is to illustrate, yet from another perspective, that the Beltrami Hilbert horizon, $R = r$, is an event horizon, although, in this case, of a very limited nature. Indeed this happens. First, the spacetime here, in the limit, becomes two copies

TABLE III. Quantification of how good it is to approximate the Hilbert horizon of the hyperbolic pseudosphere spacetime with a BTZ black hole event horizon. The closer $\zeta_{\text{Hyp}} \equiv (\mathcal{R}_{\text{Hh}} - \mathcal{R}_{\text{Eh}})/\mathcal{R}_{\text{Eh}}$ is to zero, the better is the approximation. We indicate three values of ℓ/r comparable to those used in Tables I and II, the corresponding values of ζ_{Hyp} , and how close the Hilbert horizon of this spacetime [$R = r\sqrt{1 + (\ell^2/r^2)}$] is to the Hilbert horizon of the Beltrami spacetime ($R = r$) (that is also a measure of how well the hyperbolic pseudosphere spacetime can be identified with the Beltrami spacetime). In the last column are the values of the BTZ mass M in terms of graphene parameters. All the values are approximate.

ℓ/r	ζ_{Hyp}	$(R_{\text{Hh}} - r)/r$	M
0.1	5×10^{-3}	5×10^{-2}	10^{-2}
10^{-4}	5×10^{-9}	5×10^{-5}	10^{-8}
10^{-7}	5×10^{-15}	5×10^{-8}	10^{-14}

of the Beltrami spacetimes (see previous discussion, and Fig. 10). Second, although $\mathcal{R}_{\text{Eh}} \rightarrow \mathcal{R}_{\text{Hh}} \rightarrow 0$, this corresponds to a nonzero Hilbert horizon for the hyperbolic pseudosphere spacetime, $R_{\text{Hh}} \rightarrow r$, that in turn coincides with the Hilbert horizon of the Beltrami spacetime. Here we have two such horizons (see Fig. 10), a situation that evokes a wormhole.

Some last comments are in order. The definition (B8) of the cosmological constant gives a very large negative value, $\Lambda = -1/\ell^2 \simeq -2.5 \times 10^{19} \text{ m}^{-2}$. This makes it less appealing for cosmological considerations than the definition $\Lambda = +1/r^2$, used in the de Sitter/elliptic pseudosphere case. On the other hand, that definition makes justice of our *Ansatz* that relates c to what sets the length scale of the given spacetime, especially in this case where the mass is a dimensionless parameter. It must be clear, though, that the BTZ spacetime we have briefly evoked here is not what we have when we shape graphene as a hyperbolic pseudosphere, but it is only related to it through (B7). Hence, the identification $\Lambda = -1/\ell^2$, which points to a Ricci scalar curvature of $-6/\ell^2$, should not create confusion. The latter is the Ricci curvature of the Weyl-related BTZ spacetime, while the Ricci curvature of the hyperbolic pseudosphere spacetime is $-2/r^2$.

- [1] P. W. Anderson, *Phys. Rev.* **130**, 439 (1963).
 [2] T. W. B. Kibble, *Scholarpedia* **4**, 6441 (2009).
 [3] D. Gerace and I. Carusotto, *Phys. Rev. B* **86**, 144505 (2012); A. Fabbri, *J. Phys. Conf. Ser.* **314**, 012029 (2011); R. Balbinot, I. Carusotto, A. Fabbri, and A. Recati, *Int. J. Mod. Phys. D* **19**, 2371 (2010); A. Recati, N. Pavloff, and I. Carusotto, *Phys. Rev. A* **80**, 043603 (2009).

- [4] J. Maldacena, in *Black Holes in Higher Dimensions*, edited by G. T. Horowitz (Cambridge University Press, Cambridge, UK, 2012).
 [5] K. S. Novoselov, A. K. Geim, S. V. Morozov, D. Jiang, Y. Zhang, S. V. Dubonos, I. V. Gregorieva, and A. A. Firsov, *Science* **306**, 666 (2004).
 [6] A. K. Geim, *Science* **324**, 1530 (2009).

- [7] A. H. Castro Neto, F. Guinea, N. M. R. Peres, K. S. Novoselov, and A. K. Geim, *Rev. Mod. Phys.* **81**, 109 (2009).
- [8] A. Iorio, *Ann. Phys. (Amsterdam)* **326**, 1334 (2011).
- [9] A. Iorio and G. Lambiase, *Phys. Lett. B* **716**, 334 (2012).
- [10] A. Iorio, *Eur. Phys. J. Plus* **127**, 156 (2012).
- [11] A. Iorio, *J. Phys. Conf. Ser.* **442**, 012056 (2013).
- [12] A. Iorio, L. O’Raifeartaigh, I. Sachs, and C. Wiesendanger, *Nucl. Phys.* **B495**, 433 (1997).
- [13] L. P. Eisenhart, *A Treatise on the Differential Geometry of Curves and Surfaces* (Princeton University Press, Princeton, NJ, 1909).
- [14] D. Hilbert and S. Cohn-Vossen, *Geometria Intuitiva* (Boringhieri, Torino, 1972); Italian translation of D. Hilbert and S. Cohn-Vossen, *Anschauliche Geometrie* (Julius Springer, Berlin, 1932).
- [15] A. Ovchinnikov, in *Nonlinearity and Geometry*, edited by D. Wójcik and J. Cieřliński (Polish Scientific Publishers PWN, Warsaw, 1998), pp. 41–60.
- [16] M. Bañados, C. Teitelboim, and J. Zanelli, *Phys. Rev. Lett.* **69**, 1849 (1992).
- [17] M. Bañados, M. Henneaux, C. Teitelboim, and J. Zanelli, *Phys. Rev. D* **48**, 1506 (1993).
- [18] S. Carlip, *Classical Quantum Gravity* **12**, 2853 (1995).
- [19] A. Iorio, *Alternative Symmetries in Quantum Field Theory and Gravity* (Charles University Habilitation, Prague, 2011).
- [20] M. Blasone, P. Jizba, and G. Vitiello, *Quantum Field Theory and its Macroscopic Manifestations* (Imperial College Press, London, 2011).
- [21] N. D. Birrell and P. C. W. Davies, *Quantum Fields in Curved Space* (Cambridge University Press, Cambridge, 1982); R. W. Wald, *Quantum Field Theory in Curved Spacetimes and Black Hole Thermodynamics* (The University of Chicago Press, Chicago, 1994); S. A. Fulling and S. N. M. Ruijsenaars, *Phys. Rep.* **152**, 135 (1987).
- [22] S. Takagi, *Prog. Theor. Phys. Suppl.* **88**, 1 (1986).
- [23] W. Israel, *Phys. Lett.* **57A**, 107 (1976).
- [24] A. Iorio, A. Capolupo, G. Lambiase, and G. Vitiello (work in progress).
- [25] K. S. Gupta and S. Sen, *Phys. Rev. B* **78**, 205429 (2008).
- [26] H. A. Kastrop, *Fortschr. Phys.* **51**, 975 (2003).
- [27] R. Derco, M.Sc. thesis, Charles University, Prague, 2011.
- [28] A. Iorio, *Weyl Symmetry in Graphene*, Lecture Notes at the Workshop “Modeling Graphene-like Systems,” (University College Dublin, Ireland, 2014).
- [29] M. Cvetič and G. W. Gibbons, *Ann. Phys. (Amsterdam)* **327**, 2617 (2012).
- [30] G. Guralnik, A. Iorio, R. Jackiw, and S.-Y. Pi, *Ann. Phys. (Amsterdam)* **308**, 222 (2003).
- [31] P. R. Wallace, *Phys. Rev.* **71**, 622 (1947).
- [32] G. W. Semenoff, *Phys. Rev. Lett.* **53**, 2449 (1984).
- [33] J. C. Meyer, A. K. Geim, M. I. Katsnelson, K. S. Novoselov, T. J. Booth, and S. Roth, *Nature (London)* **446**, 60 (2007).
- [34] QFT Aspects of Condensed Matter Physics, Workshop, 2011, Frascati, <http://agenda.infn.it/conferenceDisplay.py?confId=3805>.
- [35] D. Malko, C. Neiss, F. Viñes, and A. Görling, *Phys. Rev. Lett.* **108**, 086804 (2012).
- [36] J. Gonzalez, F. Guinea, and M. A. H. Vozmediano, *Phys. Rev. Lett.* **69**, 172 (1992); *Nucl. Phys.* **B406**, 771 (1993).
- [37] F. de Juan, A. Cortijo, and M. A. H. Vozmediano, *Phys. Rev. B* **76**, 165409 (2007).
- [38] R. Penrose, *The Road to Reality* (Knopf, New York, 2005).
- [39] N. M. R. Peres, *Rev. Mod. Phys.* **82**, 2673 (2010).
- [40] A. Cortijo and M. A. H. Vozmediano, *Europhys. Lett.* **77**, 47002 (2007); A. Cortijo and M. A. H. Vozmediano, *Nucl. Phys.* **B763**, 293 (2007).
- [41] H. Kleinert, *Gauge Fields in Condensed Matter* (World Scientific, Singapore, 1989), Vol. II.
- [42] M. O. Katanaev and I. V. Volovich, *Ann. Phys. (N.Y.)* **216**, 1 (1992).
- [43] M. A. H. Vozmediano, M. I. Katsnelson, and F. Guinea, *Phys. Rep.* **496**, 109 (2010).
- [44] F. Guinea, B. Horowitz, and P. Le Doussal, *Phys. Rev. B* **77**, 205421 (2008); F. Guinea, M. Katsnelson, and M. A. H. Vozmediano, *Phys. Rev. B* **77**, 075422 (2008); F. Guinea, A. Geim, M. Katsnelson, and K. Novoselov, *Phys. Rev. B* **81**, 035408 (2010).
- [45] N. Levy, S. A. Burke, K. L. Meaker, M. Panlasigui, A. Zettl, F. Guinea, A. H. Castro Neto, and M. F. Crommie, *Science* **329**, 544 (2010).
- [46] A. Iorio and P. Pais, (in preparation).
- [47] F. de Juan, M. Sturla, and M. A. H. Vozmediano, *Phys. Rev. Lett.* **108**, 227205 (2012).
- [48] R. McLachlan, *Math. Intell.* **16**, 31 (1994).
- [49] M. Spivak, *A Comprehensive Introduction to Differential Geometry, Part III* (Publish or Perish Inc., Houston, 1999).
- [50] P. A. Horvathy and J.-C. Yera, *Lett. Math. Phys.* **46**, 111 (1998).
- [51] N. Hitchin, *Geometry of Surfaces*, Lecture Notes at Oxford University (2004), <http://www.maths.ox.ac.uk/system/files/coursematerial/2013/2377/9/notes2013.pdf>.
- [52] R. M. Wald, *General Relativity* (The University of Chicago Press, Chicago, 1984).
- [53] R. d’Inverno, *Introducing Einstein’s Relativity* (Oxford University Press, Oxford, 1992).
- [54] I. Booth, *Can. J. Phys.* **83**, 1073 (2005).
- [55] M. Giovannini, *A Primer on the Physics of the Cosmic Microwave Background* (World Scientific, Singapore, 2008).
- [56] S. Deser and O. Levin, *Phys. Rev. D* **59**, 064004 (1999); *Classical Quantum Gravity* **14**, L163 (1997).
- [57] A. Capolupo, M. Di Mauro, and A. Iorio, *Phys. Lett. A* **375**, 3415 (2011); A. Capolupo and M. Di Mauro, *Phys. Lett. A* **376**, 2830 (2012).
- [58] F. Acerbi, G. Morchio, and F. Strocchi, *J. Math. Phys. (N.Y.)* **34**, 899 (1993).
- [59] M. K. Parikh and F. Wilczek, *Phys. Rev. Lett.* **85**, 5042 (2000).
- [60] F. Tung, M. Yoshimura, and K. Ueda, *J. Nanomater.* **2009**, 612549 (2009).
- [61] A. Altland and B. Simons, *Condensed Matter Field Theory* (Cambridge University Press, Cambridge, UK, 2006).
- [62] W. G. Unruh, *Phys. Rev. D* **14**, 870 (1976).
- [63] N. Nicolaevici, *Prog. Theor. Phys.* **127**, 433 (2012).
- [64] K. Ohnishi and S. Takagi, *Prog. Theor. Phys.* **88**, 895 (1992).